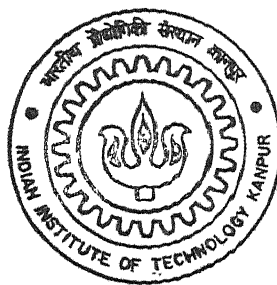


EFFECT OF TIP SWEEP ON THE PERFORMANCE OF HELICOPTER ROTOR IN HOVER

by

Anugu Prabodhan

TH
AE/2002/M
P88c



DEPARTMENT OF AEROSPACE ENGINEERING
Indian Institute of Technology Kanpur

AUGUST, -2002-

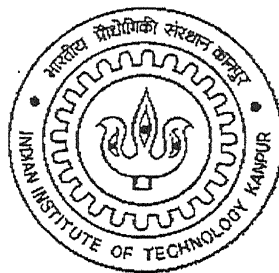
EFFECT OF TIP SWEEP ON THE PERFORMANCE OF HELICOPTER ROTOR IN HOVER

A thesis submitted
in partial fulfillment of the requirements
for the degree of

Master of Technology

by

ANUGU PRABODHAN



**DEPARTMENT OF AEROSPACE ENGINEERING
INDIAN INSTITUTE OF TECHNOLOGY, KANPUR**
August 2002

12 MAY 2003

पुरुषोत्तम
भारतीय
अवधि क्र० A.

कागज

कानपुर



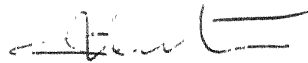
A143417



CERTIFICATE

It is certified that the work contained in the thesis titled **“EFFECT OF TIP SWEEP ON THE PERFORMANCE OF HELICOPTER ROTOR IN HOVER”**, by **ANUGU PRABODHAN**, Roll No. Y010117, has been carried out under my supervision and that this work has not been submitted elsewhere for a degree.

August 2002



Dr. C.VENKATESAN

Professor

Department of Aerospace Engineering

Indian Institute of Technology.

Kanpur

ACKNOWLEDGEMENT

I am extremely grateful to Prof. C. Venkatesan, my thesis supervisor for his constant support and guidance throughout this work. His valuable suggestions and critical remarks helped me a lot in completing this work successfully. I would also like to specially thank Dr. D.Yadav and Dr. C.S.Upadhyay, who helped create a congenial workplace, self-sufficient in infrastructure, which has made life easier for students.

I am very thankful to Mr. Rohin and Mr. Mohite for their suggestions and help throughout this work. Special thanks to Pavan, Uma, Padamata and Srilu for their help throughout this work.

I would like to thank all my colleagues and friends at structural analysis lab for their cooperation and help. I am very much thankful to A.S.Rao, Raja, Sravan, Vaitla, Mallesh, Atul, amanaya, Behara, Dhanu and to my juniors Venu, Nag, Anu, Chandu, K.S.V., Sridhar, Rajesh and nandu who make life at IITK a memorable experience.

Words are not enough to explain my feelings towards my parents, my uncles Narendhar Reddy, Pratap Reddy and brother Sudhakar Reddy. They have always been the constant source of inspiration for me.

Anugu Prabodhan

August 2002

CONTENTS

NOTATIONS

ABSTRACT	5
1) INTRODUCTION	6
1.1. GENERAL.....	6
1.2. ROTOR AERODYNAMICS.....	8
1.2.1. Hover.....	8
1.3. INTRODUCTION TO TIP SHAPES.....	10
1.4. EXISTING THEORIES OF ANALYSIS.....	12
1.5. OBJECTIVES OF THE PRESENT STUDY.....	15
2) MATHEMATICAL MODELLING	16
2.1. DESCRIPTION OF THE PROBLEM AND THE METHOD CHOSEN...	16
2.2. ASSUMPTIONS.....	17
2.3. FORMULATION.....	18
2.3.1. Coordinate Equations Used.....	18
2.3.2. Biot-Savart Law.....	21
2.3.3. Derivation for Tip-Vortex Induced Velocity Expressions.....	22
2.3.4. Derivation for Inboard Vortex Sheet Induced Velocity Expressions..	24
2.3.5. Derivation for Far Wake Induced Velocity Expressions.....	25
2.3.6. Derivation for the Induced Velocity Expressions Due to Other Lifting Lines.....	27
2.3.7. Lifting Line Theory Expressions.....	28
2.3.8. Performance Parameters Derivation.....	30

3) SOLUTION METHODOLOGY.....	32
3.1. METHODOLOGY.....	32
3.2. ALGORITHM OF THE CODE.....	34
4) RESULTS AND DISCUSSIONS.....	35
4.1. VALIDATION FOR FIXED WING.....	35
4.2. CALCULATIONS FOR THE RECTANGULAR ROTOR BLADE...	35
4.3. CALCULATIONS FOR THE SWEPT TIP ROTOR BLADE.....	37
5) CONCLUSIONS.....	39
6) SUGGESTIONS FOR FUTURE WORK.....	40
7) APPENDIX.....	41
8) REFERENCES.....	43
9) FIGURES.....	46

NOTATIONS

a	:	lift slope curve
c	:	chord of the rotor blade
C_L	:	coefficient of lift
C_D	:	coefficient of drag
C_T	:	thrust coefficient of the blades
C_Q	:	moment coefficient of the blades
k	:	tip-vortex settling rate before it passes the adjacent blade
k_2	:	tip-vortex settling rate after it passes the adjacent blade
l	:	lift per unit span
N	:	number of blades
r	:	radial location of the vortex
r_A	:	radial location on the blade from which the vortex emerges
r_c	:	root cutout
R	:	radius of the rotor blade
u	:	velocity of the flow at the section due to the blade rotation
v_h	:	mean induced velocity in hover
v_x	:	x-component of the induced inflow
v_z	:	z-component of the induced inflow
V_∞	:	axial velocity of the rotor
W	:	net-inflow on the blade
α	:	effective angle of attack of the blade section
β	:	induced angle at the blade section
Γ	:	blade circulation
Γ_t	:	tip-vortex circulation
λ	:	wake contraction parameter
λ_t	:	normalized total inflow
λ_c	:	normalized axial flow

λ_i	:	normalized induced velocity
μ	:	ratio of the drag and lift coefficients
θ	:	total angle of attack at the blade section
θ_0	:	pitch of the blade
θ_1	:	total twist in the blade in degrees(tip angle - root angle)
ρ	:	density of air
σ	:	blade solidity (total blade area / rotor disk area)
Ω	:	angular velocity of the blade
ψ_w	:	wake azimuth angle

ABSTRACT

Helicopter rotors operate in complex aerodynamic environment comprising of several significant fluid dynamic phenomena like blade-vortex interactions, reverse flow and stall on the retreating blade, formation of shockwaves and other compressibility effects on the advancing blade, and radial flow. This makes the rotor airloads calculation a difficult problem. Several aerodynamic models have been developed, starting from simple momentum theory, blade element theory, vortex theory to more complex CFD methods. Of these combined blade element-momentum theory is widely used for most of aeroelastic studies, because of its simplicity. However vortex methods are used for airloads computation. The aim of this study is to develop a prescribed wake vortex model to predict the performance of rotor blades.

Earlier, a model based on the vortex theory was developed for rotor airloads calculation for a rectangular straight blade in hover. In the present analysis it is further improved to accommodate the effect of tip sweep. The effect of swept tip on aerodynamic performance characteristics are calculated and compared with those of straight rectangular blade results. It is observed that (aft sweep) reduction in rotor power, which has been observed in experimental studies.

Chapter 1

INTRODUCTION

1.1. GENERAL

A helicopter differs from an aeroplane in the sense that it can hover, take-off and land vertically, which makes it an extremely useful flying machine in times of distress or war. Because of the very demanding maneuvers it is expected to perform, the helicopter is a machine of considerable mechanical and aerodynamic complexity. This can be gauged from the slow progress in its development as compared to that of the aeroplane. Helicopters have come a long way from the noisy Gyroplanes and Sikorskys of the early 20th century to the sophisticated Apaches. This could be made possible only through sustained research, which has led to improved performance, lift capability, and reliability. Since the 80s there has been an accelerated effort towards understanding and overcoming some of the technical, especially, aerodynamic problems in helicopter flight. With the rapid progress in processing speeds of computers, CFD techniques- mostly Euler and Navier-Stokes codes, are being applied to areas, which were, previously, unsolvable through traditional theories.

Rotor airloads calculation is an aeroelastic problem. It involves the calculation of aerodynamic forces and the resulting rotor response iteratively. In forward flight, the difference in the velocities in the advancing and retreating sides cause a 1/rev variation in the aerodynamic environment, which means that the loading and the resulting response of the blades will be periodic. The 1/rev variation in velocities causes a rolling moment and hence very large 1/rev structural loads at the root of the blade. To counter these loads by aerodynamic forces, flap and lag motions are allowed. Pitch motion is allowed for blade control and elastic torsion motion occurs due to blade torsion flexibility. Elastic torsion motion changes the blade angle-of-attack, and thus affects the airloads significantly. It is

seen that, in general, the influence of structural dynamics on the calculated airloads is comparable to the influence of rotor wake effects, as is characteristic of aeroelastic problems.

It can be seen that rotor airloads calculation is an extremely difficult problem and it is the belief of some researchers that not much progress has been made in this area. Bousman¹ delves into this aspect in a recent paper. He notes that, in rotor loads calculation, some of the present day analyses compute the magnitude of the critical design loads in maneuvers, correctly; but they fail to give the correct phase, which indicates that there is a deficiency in modeling of the physics involved. One such unsolved problem is the inability of the analyses to predict the negative lift in high-speed flight (Fig. 1). Another significant barrier to progress in the prediction of loads and vibration is the inability of the lifting-line analyses to predict the section pitching moments and hence the resulting control system loads (Fig. 2).

The analytic method for rotor loads calculation can be summarized by the flow diagram given by Sadler², Fig. 3. One set of the model deals with the wake model and associated calculations; the other deals with the determination of the aerodynamic blade loads and response.

The flow field³ of helicopter rotors is extremely complex, as can be seen from Fig. 4. It comprises of several significant fluid dynamic phenomena like strong tip vortices, blade-vortex interactions, reverse flow and stall on the retreating blade, formation of shockwaves and other compressibility effects on the advancing blade, and radial flow. All these phenomena have significant effects on rotor performance, loads and vibration. For an accurate comprehensive analysis, all these features are to be included.

Bousman¹, in his paper, states that since the present day analytical methods do not consistently and accurately predict the loads and vibration of a rotorcraft, it is not possible to determine the relative importance of the various aspects involved in the modeling, like the rotor wake, unsteady aerodynamics, radial flow and elastic deformations of the blade. He, also, concludes that for the correct prediction of the loads and vibration, it is important that all the features be properly represented.

1.2. ROTOR AERODYNAMICS

The helicopter uses its rotating wings to provide for lift, propulsion and control forces. Major differences in the aerodynamic characteristics of a rotor from those of fixed wings are:

1. High concentration of bound circulation over the outer portion of the blade resulting in an intense vortex trailed from the tip.
2. A curved spiraling wake, which initially remains close to the rotor causing strong blade/vortex interactions.
3. time dependency of stall and compressibility effects on the blade.

Helicopter motion is of three types:

1. Hover :

In this state, the rotor has no vertical or sideways velocity relative to air.

2. Axial flight :

In this state, the helicopter moves only vertically.

3. Forward flight:

In this state, there is, only, horizontal movement of the helicopter.

Only *hover* state have been consider in the present analysis.

1.2.1. Hover

Figure5 shows the schematic of the wake for one blade, from the flow visualization results of Gray⁴ for hovering condition. As can be seen, the most dominant flow feature in the helicopter flow field are the strong vortices trailed at the tips of each blade which occur due to the concentrated lift and circulation there. Figure6 shows the visualization of the tip vortex shed⁵ by a blade. It is clearly showing the contraction and the convection of the tip vortex of one blade.

The calculations of Clark and Leiper clearly show the wake feature⁶ found experimentally by Landgrebe⁴, namely, that the outer trailing vortices roll up quickly to form a strong tip vortex, while the inner vortices move downwards as a vortex sheet which becomes progressively more inclined to the rotor plane. Figure 7 shows the results of such calculations for the six-bladed CH-53A rotor. They also find that the initial position of the tip vortex depends strongly on the number of blades, if the number of blades is high, the tip vortex remains roughly in the plane of the rotor until it becomes close to the succeeding blade, when it is convected downwards.

The other feature is the inboard vortex sheet of trailed vorticity, with opposite sign as the tip vortex. The axial velocity of the outer end of the inboard vortex sheet is greater than the tip vortex with the result that they separate. Also, the inclination of the inboard vortex sheet is due to the varying axial velocity along the radius. The aggregate of similar wake structures of all the blades of the rotor make up the complete wake representation.

It is seen in Fig. 5 that successive turns of the tip-vortex remain a fixed distance away from each other. Also, the tip-vortex trajectory is taken to be a smoothly contracting semi-infinite cylindrical surface. This is, however, only a simplified illustration of the very complex nature of the rotor wake. Experiments have shown the far wake to be unstable⁴. It was also seen that the tip-vortices from adjacent blades merge^{7, 8}. Jain and Conlisk⁹ have shown this in their computations also. The interaction, which occurs in the region of maximum wake contraction, results in core breakdown followed by the diffusion of vorticity. This causes the wake to expand and hence there is a redistribution of vorticity in this region, which is close enough to the blade to induce significant inflow on the rotor. The said interaction was found to occur near the wake azimuth corresponding to the fourth tip vortex passage below the reference blade irrespective of the number of blades of the rotor. In order to make up for this additional source of inflow, Kocurek and Tangler⁷ proposed a vortex ring of radius equal to the rotor radius and at the axial level corresponding to the fourth tip vortex passage beneath the reference blade. Its strength was taken to be equal to four times that of the tip vortex. (Fig. 8). In recent study the vortex model¹⁰ (Fig. 9) used for calculation during pitch up

motion. The vortex wake is represented by the group of concentric and coplanar vortex rings representing the evolution of the circulation along the blade with azimuth.

1.3. INTRODUCTION TO TIP SHAPES

The tips of the blades play a very important role in the aerodynamic performance of the rotor. The blade tips encounter the highest dynamic pressure and highest Mach number, and strong trailed tip vortices are produced there. Figure 10 shows various blade tip designs¹¹ that have been used or proposed for helicopter rotors. There are several common designs, comprising those with taper, those with sweep, and those with a combination of sweep and taper. Some blade tips may also use an anhedral. Sweeping the leading edge of the blade reduces the Mach number normal to the leading edge of the blade, so allowing the rotor to attain a higher advance ratio before compressibility effects manifest as an increase in power required. However, the problem of rotor tip vortex formation and the effects of tip shape on the vortex characteristics such as velocity profile and diffusive characteristics is, however, still the subject of ongoing research.

McVeigh and McHugh¹² have conducted experiments with subscale rotors to study the effects of tip shapes on overall rotor performance and cruise lift-to-drag ratio. It was shown that the combined use of improved airfoil sections and tapered tip shapes can help minimize profile power and significantly improve rotor cruise efficiency. The effects of tip shapes were examined for four rotors having rectangular, swept, swept-tapered, and tapered tips. All rotors were tested at the same lift, propulsive force, and trim state, which provides a datum for performance comparisons. The tapered tip is found to give about 10% higher equivalent L/D compared to the rectangular blade, but interestingly enough the rectangular blade gives a better maximum cruise L/D than either of the swept or swept tapered blades. This is because both the advancing and retreating blade characteristics of the tip shape are important, and an integrated performance metric such as L/D does not allow to distinguish separately between these characteristics. While sweepback alone clearly has the advantage of delaying the onset of compressibility effects to higher advanced ratios, the sweep may also promote early flow separation on

the retreating blade at lower angle of attack. Therefore there can also be a performance penalty associated with a swept tip.

Various types of tip shapes including rectangular, tapered, swept rectangular, and swept tapered were discussed thoroughly¹³. Extensive research has been conducted in recent years to further quantify the benefit of various tip shapes. The following observations were found in the literature.

Thomas H. Maier¹⁴ studied the aeroelastic stability of straight and swept tip rotor plates. A planform view of the blades is shown in Fig .11. The swept tip blade has 30° of sweep which starts at 90% span. He found that for straight blades the flap, lag frequencies were slightly higher and torsion frequency was slightly lower than the swept-tip blades.

The BERP (British Experimental Rotor Program) rotor blade is also a special type rotor because of its unique tip shape (Fig.12.). This rotor was designed specifically to meet the conflicting aerodynamic requirements of the advancing and retreating blade conditions, either of which can limit the performance of the rotor in high-speed forward flight. However, the aerodynamic improvements shown with the BERP rotor are the result of several innovations in both airfoil design and tip shape design. One of the most recognizable features of the BERP blade is the use of high sweepback over the tip region. It reduces the compressibility effects and delays their effects on the rotor to a higher advance ratio. The BERP rotor is specially to perform as a swept tip at high Mach numbers and low angles of attack, but it is also designed to operate at very high angles of attack without stalling. The design of BERP rotor attempts to reduce compressibility effects on the advancing blade while simultaneously delaying the onset of retreating blade stall.

Wind tunnel tests of a rotor were conducted¹⁵ to determine the effects on dynamic response and aerodynamic performance by varying the tip design of the outboard 8% radius. Four different blade tip geometries or shapes having different planform, sweep, taper, and anhedral were tested. Results from the tests showed that blade torsional moments and control forces were reduced by adding sweep or anhedral. The anhedral tip benefited hover performance while the swept/taper tip provided the best performance at high advance ratios.

Another wind tunnel test¹⁶ was conducted to measure the aerodynamic benefit of a parabolic swept-back tip with anhedral on a 3-bladed model rotor equipped with very rigid blades. The swept onset was at 90% radius. Significant improvements on hover and forward flight performance and noise reduction over a rectangular planform were achieved.

A test of a full scale rotor¹⁷ was conducted for the four tips (rectangular, tapered, swept rectangular, and swept/tapered) shown in Fig.13, which were interchangeable over the outer 5% radius. All tips used a 9.5% airfoil. Data showed that the tapered planform had the largest impact on the overall performance while sweep effect was secondary.

1.4. EXISTING THEORIES OF ANALYSIS

The task of the aerodynamic analysis of the rotor blade is to find the induced velocity and performance characteristics for a given thrust. Aerodynamic models used in comprehensive analysis of the helicopter rotors have evolved from the simple *momentum theory* based on a uniformly loaded actuator disk through the *classical blade element-momentum method* and *wake modeling* procedures to *CFD methods* which developed in pace with the high speed digital computer.

Momentum theory applies the basic conservation laws of fluid mechanics (conservation of mass, momentum and energy) to the rotor and the flow as a whole to estimate the rotor performance. It is a global analysis, relating the overall mean flow velocities and the total rotor thrust and power. The rotor is assumed to be composed of an infinite number of blades and operates in an incompressible frictionless fluid. *Momentum theory* provides a fast, convenient means of predicting overall performance, but is not concerned with the details of rotor loads or flow and hence alone is not sufficient for designing the rotor blades.

Blade element theory calculates the forces on the blades due to its motion through the air, and hence the forces and performance of the entire rotor. Basically, blade element theory is *lifting-line theory* applied to the rotating wing. Each section of the blade is assumed to act as a two-dimensional airfoil to produce aerodynamic forces, with the influence of the wake and the rest of the rotor contained entirely in the induced angle of

attack at the section. The solution thus requires an estimate of the wake-induced velocity at the rotor disk, which is provided by *momentum theory*, *vortex theory*, or *combined blade-element/momentum theory*.

Vortex theory is a rotor analysis that calculates the flow field of the rotor wake and the induced velocity at the rotor disk by using the fluid dynamic laws governing the action and influence of vorticity (the Biot-Savart law, Kelvin's theorem, and Helmholtz's laws). This theory uses *lifting line* or *lifting surface* theories together with a wake model for the performance calculations. The wake geometry is taken to be either the reliable, easy-to-use *prescribed wake* or the sophisticated and computationally demanding *free wake*.

In the *prescribed-wake analysis*, the geometry of the vortex sheets from the individual blades are prescribed in advance, which implies that the velocity field has been assumed. In this approach, the wake geometry is specified as a function of rotor configuration and thrust level through simple analytical expressions.

Landgrebe⁴ demonstrated the practicality of this method by incorporating an experimentally derived generalized wake description in the UTRC Prescribed Wake Hover Performance Analysis. Kocurek and Tangler⁷ used a *prescribed wake lifting surface* model in their performance analysis.

In the *free-wake analysis*, an initial distribution of the vortex sheets is assumed and the elements of the vortex sheets are allowed to convect in the velocity field they create. The vortex elements will move until they take up positions, which are consistent with the velocity field. This analysis requires orders of magnitude more computation than the prescribed wake. Application of the *free-wake analysis* can be found in the works of Sadler², and Bagai and Leishman¹⁸.

Prescribed wake does not give good results in low speed forward flight while *free wake* does. But the importance of the *free wake* declines as airspeed increases and at high speeds, there is no difference in the two wake models.¹

Lifting line theory is based on the assumption that the wing has a high aspect ratio, which is, in general, valid for a helicopter rotor wing. However, in areas where the loading or induced velocity has high gradients such as the sections near the tip or near an encounter with a vortex from a preceding blade, *lifting line theory* may not be accurate.

This model usually gives high gradients in induced velocity when the tip vortex passes close to the tip. Lifting line formulation neglects all planform effects.

In second-order lifting line theory^{19,20} each blade is divided into a finite number of span-wise segments with a span-wise bound vortex located at the quarter chord line and a control point placed at the middle of three-quarter chord line in each segment. The wake vortex filaments are trailed from the trailing edge of the blade. Hence, there are the so-called chord-wise bound vortices between the lifting line and the trailing edge. In this assumption, the close encounter of the trailing vortices with the control points can be effectively avoided during the solution. *Second order lifting line theory*²⁰ has given results same as *lifting surface theory* and can be used to improve the calculation of airloads instead of resorting to the computationally demanding *lifting surface* or *CFD methods*.

Lifting surface analysis is required for an accurate treatment of the vortex-induced loads on a rotor blade, especially for extremely small vortex-blade separations where the loading varies greatly in a short distance along the blade. This theory represents the wing by vortex surfaces and satisfies the boundary conditions over the entire surface. It can handle the large variations of induced velocity and loading that occur at the blade tip or in an encounter with a wake vortex. In Kocurek and Tangler's model⁷, the rotor *lifting surface* is developed from a "Vortex-Box" surface and wake numerical model.

Lifting surface analysis would be beneficial for any planform which varies significantly from the conventional, constant chord, blade. A sensible compromise between accuracy and computational effort would be to provide a single panel lifting surface model in rotor applications. The full *lifting surface* model may be used where a more detailed accounting of both planform and wake influences on the blade is needed.

Baskin et al²² give a very thorough exposition of the application of the *vortex theory* to rotary-wing aerodynamics in their book. Johnson¹⁹⁻²¹ provides a detailed comprehensive analysis of rotor wings based on the vortex methods and also an overview of some of the methods used for a comprehensive analysis.

Potential theory finds the induced velocity by solving the fluid dynamic equations for the velocity or stream function. It requires the assumptions that the flowfield is inviscid, irrotational, and isentropic. Application of velocity and acceleration potentials

makes it possible to determine steady and unsteady flow fields induced by the rotor in both incompressible and compressible fluids with a precision similar to that offered by the vortex theory approach but with less computational effort. Mangler and Squire were one of the first to adapt the velocity and acceleration potential concepts to the rotor for finding the induced velocity field. *Rotary wing Aerodynamics*²³ gives a brief outline of the application of *potential theory* to the determination of flow fields around three-dimensional, non-rotating bodies.

Some of the current methods of CFD^{24,25} used for calculating rotor performance solve the *potential*, *Euler* or *Navier-Stokes* equations coupled with an external *free-* or *prescribed-wake* model based on the *lifting line* or *lifting surface theory*. These approaches require fairly large computer resources from solving two coupled models simultaneously. The other approaches are the *CFD wake capturing methods*, wherein the entire flow field is simulated with a unified differential method. No wake model is used, provided the grid contains the whole domain. For the rotor in hover, *CFD methods* have been used for *Euler computations* or *Navier-Stokes computations* with different strategies like embedded grids or unstructured grids. In principle, *CFD methods* may be used to compute fundamental fluid properties on both the rotor blades and the wake. However, the degree of complexity associated with the CFD schemes demand prohibitively high computational tools.

1.5. OBJECTIVES OF THE PRESENT STUDY

The objective of this study is to improve the vortex model (having prescribed wake structure) developed in Ref. [29] for rectangular blades, to include the effect of tip sweep. In order to validate the mathematical formulation and the computer code, first the aerodynamic loads on a swept fixed wing were calculated. These results are compared with the results available in the literature. Then performance of rotor blades having swept tip have been evaluated and the effects of tip sweep on rotor thrust and rotor torque have been analysed.

Chapter 2

MATHEMATICAL MODELLING

2.1. DESCRIPTION OF THE PROBLEM AND THE METHOD CHOSEN

The aim is to develop a code to carry out the performance calculations of a rotor blade with swept tip in hover state, given the rotor configurations like the number of blades, size of the blades, pitch, sweep.

Lifting line theory is used for the analysis considering the conclusion of the authors²⁶ : ‘...the lifting line approach is adequate for predicting the hover performance of a wide range of conventional and advanced rotor designs.’

The wake geometry is specified based on the semi-empirical model hypothesized by Gray and further developed by Landgrebe⁴. The equations of Landgrebe have been used as such but for the tip vortex parameters, which have been modified by Kocurek and Tangler⁷, who found Landgrebe’s generalized equations to be in disagreement with the tip vortex trajectories in their wake geometry investigations. Hence, in the final form, the tip vortex coordinates are given by Kocurek and Tangler’s recirculation model, and the geometry of the inboard wake sheet is given by Landgrebe’s wake model. The wake geometries are functions of the rotor thrust coefficient, number of blades, collective pitch angle, and blade twist.

A rotating coordinate system, fixed to the rotor and moving with it is chosen (Fig.14). Since for hover, the flow field is axisymmetric, it would be sufficient to find the loads on one blade. The results hold for all the other blades. The blade section is considered as 2-D infinite section. Conventional strip theory based on 2-dimensional airfoil data is assumed applicable to compute the rotor performance characteristics. Airfoil data has been taken from standard tables²⁷ for a *NACA 0012* blade section.

2.2. ASSUMPTIONS

Assumptions made in the analysis are:

1. A rigid rotor is assumed with constant chord case was considered.
2. Blade dynamics is not included.
3. The rotor blades are given only small pitch angles.
4. The wake is assumed to be made of line vortices, which have no core.
5. Stall and compressibility effects have not been considered.
6. Fluid dynamic characteristics of the vorticity like vortex-vortex interactions; stability of vortices; vortex core bursting and other viscous effects have not been taken into account.
7. The trailing vortices from the swept tip are also taken parallel to the trailing vortices from the straight portion of the blade.

2.3. FORMULATION

2.3.1. Coordinate Equations Used

Tip Vortex Coordinates (Fig.15a)

The generalized empirical equations⁷ (Kocurek and Tangler's model) defining the *tip vortex* axial and radial coordinates as a function of azimuth are given by,

Axial Coordinates

$$\begin{aligned} z_t &= k_1 \psi_w & 0 \leq \psi_w \leq \psi_N, \psi_N \equiv \frac{2\pi}{N} \\ z_t &= z_{t\psi_N} + k_2 (\psi_w - \psi_N) & \psi_N \leq \psi_w \leq 4\psi_N \end{aligned} \quad \text{.....(1)}$$

where z_t is the axial coordinate of the vortex

Radial Coordinates

$$r = A + (1 - A)e^{-\lambda\psi_w} \quad 0 \leq \psi_N \leq 4\psi_N \quad \text{.....(2)}$$

where A is approximately 0.78.

k_1 rate at which the vortex settles before it encounters the following blade

k_2 rate at which the vortex settles after it passes the following blade

λ wake contraction parameter

k_1 and k_2 are shown in Fig. 15a

The tip vortex trajectory equations represent the wake's structure upto the point of maximum contraction, which occurs close to a wake azimuth of $\frac{8\pi}{N}$.

Vortex Settling Rate Parameter, k_1 and k_2

$$k_1 = B + C \left(\frac{C_T}{N^n} \right)^m \quad \text{.....(3a)}$$

where

$$B = -0.000729\theta_1$$

$$C = -2.3 + 0.206\theta_1$$

$$m = 1.0 - 0.25e^{0.040\theta_1}$$

$$n = 0.5 - 0.0172\theta_1$$

θ_1 total twist in the blade (washout) in degrees

C_T Thrust Coefficient

N number of blades

$$k_2 = -(C_T - C_{T_0})^{\frac{1}{2}} \quad \text{.....(3b)}$$

where

$$C_{T_0} = N^n (-B/C)^{\frac{1}{m}}$$

Wake Contraction Parameter, λ

$$\lambda = 4.0(C_T)^{\frac{1}{2}} \quad \text{.....(4)}$$

Features:

- the axial velocity of tip vortex element is very low until it passes beneath the following blade. At that point, the tip vortex element lies radially inboard of the following blade and the induced effect of the bound and trailing vortices of that blade increase the axial displacement rate. Hence, k_2 is greater than k_1 .
- axial displacement and radial contraction of the tip vortex increase with increase in thrust level.
- For twisted rotors, the tip vortex passes above the rotor disk at low values of C_T since the tip region is producing thrust in opposition to that produced further inboard. As C_T increases to where $k_1 = 0$, there is no tip vortex and hence the tip becomes unloaded. The vortex then reappears as C_T is increased further.
- k_2 also goes to zero when $k_1 = 0$

Vortex Sheet Coordinates (Fig. 15b)

The equations for the inboard vortex sheet's axial and radial coordinates have been used without alteration from Landgrebe's model.⁴

Axial Coordinates

The inboard vortex sheet extends from the root cutout to the point where the tip vortex emerges. The axial coordinates of points on the cross sections of the vortex sheet shed by the inboard portions of the blades were approximated as varying linearly with the radius. These linear approximations are extended at both ends until they intercept the axis of rotation ($\bar{r}=0$) or an imaginary cylinder of radius ($\bar{r}=1$). Landgrebe gives the coordinates of these two end points. (Fig.15b).

$$(\bar{z}_T)_{\bar{r}=1} = \begin{cases} K_{1\bar{r}=1} \psi_w & \text{for } 0 \leq \psi_w \leq \frac{2\pi}{N} \\ (K_{1\bar{r}=1}) \frac{2\pi}{N} + (K_{2\bar{r}=1}) \left(\psi_w - \frac{2\pi}{N} \right) & \text{for } \psi_w \geq \frac{2\pi}{N} \end{cases}$$

$$\bar{z}_{\bar{r}=0} = \begin{cases} 0 & \text{for } 0 \leq \psi_w \leq \frac{\pi}{2} \\ (K_{2\bar{r}=0}) \left(\psi_w - \frac{\pi}{2} \right) & \text{for } \psi_w \geq \frac{\pi}{2} \end{cases} \quad \text{.....(5)}$$

where the vortex sheet parameters are :

$$K_{1\bar{r}=1} = -2.2\sqrt{C_T/2}$$

$$K_{2\bar{r}=1} = -2.7\sqrt{C_T/2}$$

$$K_{2\bar{r}=0} = \left[\frac{\theta_1}{128} (0.45\theta_1 + 18) \right] \sqrt{C_T/2}$$

Radial coordinates :

$$\bar{r} = \bar{r}_A \bar{r}_T \dots\dots(6)$$

where

\bar{r}_A normalized radial location of the point on the blade where the
vortex originates $= \frac{r_A}{R}$

\bar{r}_T normalized radial location of the tip vortex where it has the same
vertical displacement as that of a point on the vortex originating
from r_A

2.3.2. Biot-Savart law:

The Biot-Savart law is the basic relationship used for calculating induced flow in the vortex theory. For a line vortex with circulation Γ , the differential velocity induced, $d\vec{v}$, by a differential length of the vortex, $d\vec{l}$, is given by: (Fig. 16)

$$d\vec{v} = \frac{\Gamma}{4\pi} \frac{d\vec{l} \times \vec{r}_1}{|\vec{r}_1|^3} \dots\dots(7)$$

Sign Convention

Looking in the direction of the vortex, if the rotation of vorticity is clockwise, then $\Gamma > 0$; if the rotation is anti-clockwise, then $\Gamma < 0$.

2.3.3. Derivation for tip-vortex induced velocity expressions

Referring to Fig. 17,

Parametric equations of the tip-vortex helix

$$\begin{aligned}x_{tv} &= -r \sin \psi_w \\y_{tv} &= r \cos \psi_w \\z_{tv} &= z_t\end{aligned}\quad \text{.....(8)}$$

where

r is defined in eq. (2)

ψ_w is measured clockwise since blade rotation is anti-clockwise

Parametric equation of the lifting line of the reference blade

$$\begin{aligned}x &= -\rho \sin 0 \\y &= \rho \cos 0 \\z &= 0\end{aligned}\quad \text{.....(9)}$$

where ρ is the radial location of the reference point on the blade.

Note:

The angles have been taken zero because the lifting line of the reference blade is the line from which angles are measured.

$$\vec{r}_1 = \vec{P} - \vec{R}_1 \quad \text{.....(10)}$$

where \vec{R}_1 Vectorial position of a point on the tip vortex

\vec{P} Vectorial position of a point on the lifting line

\vec{r}_1 Vectorial position of a point on the lifting line with respect to a point on the tip vortex.

$$\vec{P} = x \hat{i} + y \hat{j} + z \hat{k}$$

where x, y, z given in eq. (9)

$$\vec{R}_1 = x_{tv} \hat{i} + y_{tv} \hat{j} + z_{tv} \hat{k}$$

where x_{tv}, y_{tv}, z_{tv} given in eq. (8)

$$\rightarrow \vec{r}_1 = (-\rho \sin 0 - x_{tv}) \hat{i} + (\rho \cos 0 - y_{tv}) \hat{j} + (-z_{tv}) \hat{k}$$

$$|\vec{r}_1| = \sqrt{(-\rho \sin 0 - x_{tv})^2 + (\rho \cos 0 - y_{tv})^2 + (-z_{tv})^2}$$

Applying Biot-Savart Law

$$d\vec{v} = \frac{\Gamma_t}{4\pi} \frac{d\vec{l} \times \vec{r}_1}{|\vec{r}_1|^3}$$

where $d\vec{v}$ is the velocity due to the infinitesimal element at any point, T, on the tip vortex

the tangential vector at T, $d\vec{l}$, is given by

$$d\vec{l} = \frac{d\vec{R}}{d\psi_w} d\psi_w = \left(\frac{dx_{tv}}{d\psi_w} d\psi_w \right) \hat{i} + \left(\frac{dy_{tv}}{d\psi_w} d\psi_w \right) \hat{j} + \left(\frac{dz_{tv}}{d\psi_w} d\psi_w \right) \hat{k}$$

$$d\vec{l} \times \vec{r}_1 = \begin{vmatrix} \hat{i} & \hat{j} & \hat{k} \\ \frac{dx_{tv}}{d\psi_w} & \frac{dy_{tv}}{d\psi_w} & \frac{dz_{tv}}{d\psi_w} \\ (-\rho \sin 0 - x_{tv}) & (\rho \cos 0 - y_{tv}) & (-z_{tv}) \end{vmatrix} d\psi_w$$

$$\vec{V} \Big|_{y_o} = \left[\int_0^{2\pi/N} d\psi + \int_{2\pi/N}^{8\pi/N} d\psi \right]$$

2.3.4. Derivation for Inboard Vortex sheet induced velocity expressions

The inboard vortex sheet originates from points on the blade lying between the root cutout ($\bar{r} = 0.1$) and the point at which the tip-vortex starts ($\bar{r} = 0.97$). The cross section of the vortex sheet at each azimuth is taken to be linear.(Fig.8). Equation (5) gives the axial displacement coordinates of the extended vortex sheet, at the points $\bar{r} = 0$ (axis of rotation) and $\bar{r} = 1$. From eq. (5), the axial coordinates for the intermediate points on the vortex sheet coordinates can be interpolated.

$$\text{if } \frac{2\pi}{N} \geq \frac{\pi}{2}$$

$$\bar{z}_i = k_{1\bar{r}=1} \cdot \psi_w \cdot \bar{r}_{Ai}$$

$$0 \leq \psi_w \leq \frac{\pi}{2}$$

$$= k_{2\bar{r}=0} \left(\psi_w - \frac{\pi}{2} \right)$$

$$\frac{\pi}{2} \leq \psi_w \leq \frac{2\pi}{N}$$

+

$$\left(k_{1\bar{r}=1} \cdot \psi_w - k_{2\bar{r}=0} \left(\psi_w - \frac{\pi}{2} \right) \right) \cdot \bar{r}_{Ai}$$

$$= k_{2\bar{r}=0} \left(\psi_w - \frac{\pi}{2} \right)$$

$$\frac{2\pi}{N} \leq \psi_w \leq \frac{8\pi}{N}$$

+

$$\left(k_{1\bar{r}=1} \cdot \frac{2\pi}{N} + k_{2\bar{r}=1} \left(\psi_w - \frac{2\pi}{N} \right) - k_{2\bar{r}=0} \left(\psi_w - \frac{\pi}{2} \right) \right) \cdot \bar{r}_{Ai}$$

.....(11)

$$\text{if } \frac{\pi}{2} > \frac{2\pi}{N}$$

$$\bar{z}_i = k_{1\bar{r}=1} \cdot \psi_w \cdot \bar{r}_{Ai}$$

$$0 \leq \psi_w \leq \frac{2\pi}{N}$$

$$= \left(k_{1\bar{r}=1} \cdot \frac{2\pi}{N} + k_{2\bar{r}=1} \left(\psi_w - \frac{2\pi}{N} \right) \right) \cdot \bar{r}_{Ai}$$

$$\frac{2\pi}{N} \leq \psi_w \leq \frac{\pi}{2}$$

$$= k_{2\bar{r}=0} \left(\psi_w - \frac{\pi}{2} \right)$$

$$\frac{\pi}{2} \leq \psi_w \leq \frac{8\pi}{N}$$

+

$$\left(k_{1\bar{r}=1} \cdot \frac{2\pi}{N} + k_{2\bar{r}=1} \left(\psi_w - \frac{2\pi}{N} \right) - k_{2\bar{r}=0} \left(\psi_w - \frac{\pi}{2} \right) \right) \cdot \bar{r}_{Ai}$$

where \bar{r}_A normalized radial location of the point on the blade where the vortex

$$\text{originates} = \frac{r_A}{R}$$

subscript i denotes the control point number on the blade

The expressions for induced velocity due to the inboard trailing vortices are similar to that derived for the tip vortex (Fig. 18).

2.3.5. Derivation for far wake induced velocity expressions

The far wake is represented by a vortex ring at a vertical distance corresponding to the fourth tip vortex passage below the reference blade. It is shown in Fig. 18.

From Biot-Savart law,

$$d\vec{v} = \frac{\Gamma_f}{4\pi} \frac{d\vec{l} \times \vec{r}}{|\vec{r}|^3}$$

where

Γ_f is the circulation of the far wake

$d\vec{v}$ is the velocity induced at P due to the

infinitesimal element at a point, T, on the vortex ring.

$$\vec{r} = \vec{P} - \vec{R}_1$$

where \vec{r} Vectorial position of a point on the lifting line with respect to a point on the vortex ring

\vec{P} Vectorial position of a point on the lifting line

\vec{R}_1 Vectorial position of a point on the vortex ring

$$\vec{R}_1 = -R_f \sin \phi \hat{i} + R_f \cos \phi \hat{j} + h \hat{k}$$

where

R_f radius of the far wake ring

h vertical distance between the blade and the far wake

$$\vec{P} = -\rho \sin 0 \hat{i} + \rho \cos 0 \hat{j} + 0 \hat{k}$$

$$d\vec{l} = \frac{d\vec{R}_1}{d\phi} d\phi = (-R_f \cos \phi \hat{i} - R_f \sin \phi \hat{j} + 0 \hat{k}) d\phi$$

where ϕ azimuthal angle of the far wake vortex element with respect to the reference blade

$$d\vec{l} \times \vec{r} = \begin{vmatrix} \hat{i} & \hat{j} & \hat{k} \\ -R_f \cos \phi & -R_f \sin \phi & 0 \\ (-R_f \sin \phi + \rho \sin 0) & (R_f \cos \phi - \rho \cos 0) & -h \end{vmatrix} d\phi$$

$$\vec{V} = \int_0^{2\pi} d\vec{v}$$

2.3.6. Derivation for the induced velocity expressions due to the other lifting lines

The bound vortices of the other blades too contribute to the induced velocity of the reference blade. (Fig. 19)

From Biot-Savart Law,

$$d\vec{v} = \frac{\Gamma(l)}{4\pi} \frac{d\vec{l} \times \vec{r}}{|\vec{r}|^3}$$

where $d\vec{l}$ vectorial element of the other bound vortex

$$\vec{r} = \vec{P} - \vec{P}_1$$

where \vec{r} is the vectorial location of a point on the reference lifting line with respect to an element of the other bound vortex

\vec{P} Vectorial position of a point on the lifting line

\vec{P}_1 Vectorial location of a point on the bound vortex

$$\vec{P} = -\rho \sin 0 \hat{i} + \rho \cos 0 \hat{j} + 0 \hat{k}$$

$$\vec{P}_1 = -\rho_1 \sin(0 + k * \pi / 2) \hat{i} + \rho_1 \cos(0 + k * \pi / 2) \hat{j} + 0 \hat{k}$$

where k blade number 0,1,2....N; 0 being the reference blade

Elemental length, dl , of the bound vortex is given by

$$\vec{l} = 0 \hat{i} + \rho_1 \hat{j} + 0 \hat{k}$$

$$d\vec{l} = 0 \hat{i} + d\rho_1 \hat{j} + 0 \hat{k}$$

$$d\vec{l} \times \vec{r} = \begin{vmatrix} \hat{i} & \hat{j} & \hat{k} \\ 0 & 1 & 0 \\ (-\rho \sin 0 + \rho_1 \sin(0 + k * \pi / 2)) & (\rho \cos 0 - \rho_1 \cos(0 + k * \pi / 2)) & 0 \end{vmatrix} d\rho_1$$

$$\vec{v} = \int_{r_c}^R \frac{\Gamma(l)}{4\pi} \frac{d\vec{l} \times \vec{r}}{|\vec{r}|^3}$$

where r_c is the root cutout and R is the radius of the blade

2.3.7. Lifting Line Theory expressions

From Fig. 20, it is seen that

$$\begin{aligned}\alpha_j &= \theta_j - \beta_j \\ &= (\theta_o + \theta_1)_j - \beta_j\end{aligned}\quad \text{.....(12)}$$

where

α_j effective angle of attack

θ_j total angle at a section

θ_o Pitch of the blade

θ_1 twist at the section

β_j induced angle at the section

subscript j number of the control point at the section

From Joukowsky's theory,

$$l = \rho W_j \Gamma_j \quad \text{.....(13)}$$

where

l lift per unit length

W_j resultant air velocity at the section

Γ_j circulation at the section

But, from experimental aerodynamics,

$$l = \frac{1}{2} C_{lj} \rho W_j^2 c_j \quad \text{.....(14)}$$

where

C_{lj} coefficient of lift at the section

ρ density of air

c_j chord at the section

From (13) and (14)

$$\rightarrow \Gamma_j = \frac{1}{2} C_{li} c_j W_j = \frac{1}{2} a_\infty \alpha_j c_j W_j \quad \text{since } C_{li} = a_\infty \alpha_j$$

a_∞ lift curve slope

$$\rightarrow \alpha_j = \frac{2 \Gamma_j}{a_\infty c_j W_j} \quad \text{.....(15)}$$

substituting in (12),

$$\frac{2 \Gamma_j}{a_\infty c_j W_j} = (\theta_o + \theta_1)_j - \beta_j$$

$$\rightarrow = (\theta_o + \theta_1)_j - \tan^{-1} \left(\frac{V_\infty + v_{zj}}{-U_j + v_{xj}} \right)$$

$$\frac{2 \Gamma_j}{a_{\infty j} c_j \left(\sqrt{(V_\infty + v_{zj})^2 + (-U_j + v_{xj})^2} \right)} = (\theta_o + \theta_1)_j - \tan^{-1} \left(\frac{V_\infty + v_{zj}}{-U_j + v_{xj}} \right) \quad \text{.....(16)}$$

where

v_{zj} vertical component of the total induced velocity

v_{xj} horizontal component of the total induced velocity

perpendicular to the blade

U_j relative velocity of air due to rotation of the blade = Ωr_j

V_∞ axial flow velocity

Eq (16) is the final form of the lifting line equation used. This is solved for Γ_j in an iterative process.

2.3.8. Performance Parameters Derivation (Fig. 20)

Consider an elemental blade segment Δr_j . As shown in Fig. 16,
The thrust per unit length,

$$F_{zj} = L_j \cos \beta_j - D_j \sin \beta_j \quad \dots\dots(17)$$

$$-F_{xj} = L_j \sin \beta_j + D_j \cos \beta_j$$

But,

$$L_j = C_{Lj} \frac{\rho}{2} W_j^2 b_j \Delta r_j \quad \dots\dots(18)$$

$$D_j = C_{Dj} \frac{\rho}{2} W_j^2 b_j \Delta r_j$$

where C_{Lj} is the lift coefficient and C_{Dj} is the drag coefficient of the airfoil

It can also be seen in Fig.20 that

$$W_j \cos \beta_j = \Omega r_j - v_{xj} \quad \dots\dots(19)$$

$$W_j \sin \beta_j = V + v_{zj}$$

substituting (15), (18), and (19) into (16) and taking $\bar{\mu}_j = \frac{C_{Dj}}{C_{Lj}}$

$$F_{zj} = \rho[(\Omega r_j - v_{xj}) - \bar{\mu}_j(V + v_{zj})]\Gamma_j \Delta r_j$$

$$-F_{xj} = \rho[(V + v_{zj}) + \bar{\mu}_j(\Omega r_j - v_{xj})]\Gamma_j \Delta r_j$$

Torque generated by the segment

$$\begin{aligned} \Delta M_j &= -F_{xj} . r_j \\ &= \rho[(V + v_{zj}) + \bar{\mu}_j(\Omega r_j - v_{xj})]\Gamma_j r_j \Delta r_j \end{aligned}$$

Total Thrust

$$T = N \sum F_{zj}$$

Total Torque

$$M = N \sum \Delta M_j$$

Coefficient of Thrust,

$$C_T = \frac{T}{\rho A (\Omega R)^2} \quad A = \pi R^2$$

$$\rightarrow C_T = \frac{N}{\pi} \sum \left[\left(\frac{r_j}{R} - \frac{v_{xj}}{\Omega R} \right) - \bar{\mu}_j \left(\frac{V}{\Omega R} + \frac{v_{zj}}{\Omega R} \right) \right] \frac{\Gamma_j}{\Omega R^2} \frac{\Delta r_j}{R}$$

$$\rightarrow C_T = \frac{N}{\pi} \sum \left[\bar{r}_j - \bar{v}_{xj} - \bar{\mu}_j (\bar{V} + \bar{v}_{zj}) \right] \bar{\Gamma}_j \Delta \bar{r}_j \quad \dots\dots(20)$$

Torque coefficient

$$C_Q = \frac{M}{\rho A R (\Omega R)^2}$$

$$\rightarrow C_Q = \frac{N}{\pi} \sum \left[\left(\frac{V}{\Omega R} + \frac{v_{zj}}{\Omega R} \right) + \bar{\mu}_j \left(\frac{r_j}{R} - \frac{v_{xj}}{\Omega R} \right) \right] \frac{\Gamma_j}{\Omega R^2} \frac{r_j}{R} \frac{\Delta r_j}{R}$$

$$\rightarrow C_Q = \frac{N}{\pi} \sum \left[\bar{V} + \bar{v}_{zj} + \bar{\mu}_j (\bar{r}_j - \bar{v}_{xj}) \right] \bar{\Gamma}_j \bar{r}_j \Delta \bar{r}_j \quad \dots\dots(21)$$

Chapter 3

SOLUTION METHODOLOGY

3.1. METHODOLOGY

The wake analysis involves two tasks - calculation of the wake-induced velocities and calculation of the resulting aerodynamic loading on the rotor blade.

Basically, the wake-induced velocity on the rotor blade is obtained by integrating the Biot-Savart law applied to the vortex elements in the rotor wake. For convenience in calculations, the wake is divided into several components – tip-vortex, inboard vortex sheet, and the far wake, which is represented by a ring vortex. There is also the contribution of the lifting lines of the blades other than the reference blade. The extent of the wake is taken to be upto an azimuth angle of $\frac{8\pi}{N}$. The wake is divided into azimuth step-sizes of 15° . The integration is done using an adaptive Simpson's rule (Appendix B) over these 15° steps.

To obtain the blade loading, the blade bound circulation variation is to be determined. This is given by the solution of Prandtl's lifting line theory. However, Prandtl's lifting line equation, being an integro-differential equation²⁸ is difficult to solve. The lifting line equation is converted into a set of algebraic equations by applying the lifting line equation to only a prescribed set of control points.

The wake from each blade is represented by a finite number of discrete vortex filaments – a strong, rolled up tip vortex filament, and several weaker filaments representing the inboard portion of the vortex sheet. The set of control points, mentioned above, are taken to be lying in between the points of origin of the vortex filaments (Fig. 21). Since the blade circulation has a larger gradient near the tip, the control points in this region are placed at closer distances than in the rest of the blade. The blade bound circulation and induced velocities are calculated at these control points. The positioning of the control points in between the vortex filaments also ensure that singularities do not occur (Fig.21). The bound circulations at the control points are the unknowns in the set

of algebraic equations obtained by applying the lifting line equation at the control points. These are solved by an iterative procedure. The difference between the bound circulations at the two adjacent control points defines the strength of trailed vorticity, which emanates between these points. Since the unknown circulations are solved iteratively, an initial estimate of the circulation would be required. For this, *combined blade-element/momentum theory* is used. The drop in circulation at the tip is, however not predicted by this theory, which is, hence, accounted for by setting the circulation to zero over a small distance at the tip.

To compute the rotor performance characteristics, 2-dimensional airfoil data²⁷ is assumed to be applicable. Lifting line theory does not predict the vortex roll-up process. However, it has been approximately modeled²⁸ by letting the discrete tip vortices to combine at an azimuth angle of 60° . The vortex wake constructed using empirical equations (section 2.3.1). The wake diagram shown in Fig.23.

3.2. ALGORITHM OF THE CODE

The algorithm for the code is given here and the flowchart of the program is given in Fig.22.

1. Rotor data is input.
2. An initial value of the blade bound vortex is estimated using the combined blade-element/momentum theory or from the value of blade circulation calculated previously for rotor configuration close to the present configuration. The strength of the trailing vortices is calculated from the blade bound circulation.
3. Next, the velocity induced at the blade by each of the wake component – tip vortex, inboard sheet, other bound vortices and the far wake- is calculated by applying the Biot-Savart law.
4. The effective angle-of-attack at each section of the blade is then calculated. Using eq. 16 (section 2.3.7), the new values of blade circulation are obtained.
5. If the new value of blade circulation is not comparable to the old value, blade circulation value is slightly increased or decreased, depending on the new value of the blade circulation.

Note: in the present analysis, the new and old values of the blade circulation are taken to be comparable if their difference is less than 0.1 times the old value of circulation. Since it is taking more time for each iteration, this assumption was made.

6. Steps 3-5 are iterated till convergence of blade circulation values.
7. Now, from the converged values of blade circulation and induced velocity values, the effective angle-of-attack, coefficient of thrust and coefficient of torque are calculated.

Chapter 4

RESULTS AND DISCUSSION

4.1. VALIDATION FOR SWEEP FIXED WING

The code was, initially, verified for the simpler case of swept tapered fixed wing since the wake consists of semi-infinite straight trailing vortices. The code was slightly modified for the swept fixed wing case but the base algorithm remained the same. The wing details are as follows:

Wing airfoil section	: NACA 65-210
Aspect ratio, AR	: 9.02
Taper ratio	: 0.4

The code results were validated with lifting surface results³⁰ for various sweep angles (as shown in Fig. 25) for different angle of attack. While increasing the angle of attack from 5° to 10° , the results were found close to lifting surface results. The lift curve for the swept tapered fixed wing was obtained and compared with the straight fixed wing results. As shown in Fig. 26, the experimental data³⁰ and the lift curve obtained from the code match to large extent, except near stall and it is also observed that the lift for swept tapered wing was slightly decreasing as compared to straight wing.

4.2. CALCULATIONS FOR THE RECTANGULAR ROTOR BLADE

The vortex model²⁹ (having prescribed wake structure) was developed for rectangular blades. The following parameters were studied.

1. Root cut-out: The lifting portion of the blade generally starts at a radial station of about 10% to 30% of the blade radius. The root cut-out was assumed as 10%.

2. Tip vortex factor (tvf): The extent of the tip region of the blade from which the tip vortices emerge (denoted as tip vortex factor, tvf). To fix the tvf, calculations for the different cases of the tvf were carried out and the value of 97% was proposed as it gave results closest to experimental data.
3. Roll-up location: After several attempts, the roll-up of the tip vortices has been chosen to occur at 60° azimuth.
4. Strength of the vortex ring: The strength of the vortex ring, which is added to make up for the additional inflow due to the diffused vorticity in the region below and outboard of the well-defined near wake. The vortex ring strength was proposed 8 times that of the tip vortex strength, for which the results are in good agreement with the experimental data.

The values proposed²⁹ for various parameters

1. Root cut-out 10%
2. Tip vortex factor (tvf) is 97 %
3. Roll-up location of tip vortices at 60°
4. Strength of vortex ring is 8 times strength of tip vortex

were used in present study. Using the above parameters, the performance calculations were carried out for a NACA 0012 rotor wing (Fig 24). The other details of the model blade configuration⁷ are given in table1. These rectangular blade results were validated with experimental data, as shown in Fig 27. It is observed that for small pitch angles the results were matching with experimental data but for large pitch angles ($>10^\circ$) this model not predicting good results.

UNTWISTED ROTOR

Aspect Ratio	N	R m(in.)	b m (in.)	ΩR m/s (fps)	Rotor solidity (σ)
18.2	4	0.679(26.75)	.037 (1.47)	152.4(500)	0.070

Table 1. Rotor Configuration used for calculations (Ref. 7)

4.3 CALCULATIONS FOR SWEPT TIP ROTOR BLADE

The sweep angle of the blade starts from 95% rotor radius. Performance calculations were carried out for swept tip rotor blade. These results are compared with straight rectangular blade results, to identify the effect of tip sweep.

Keeping the pitch angle 6° , the coefficient of thrust and torque were calculated for sweep angle varies 0° to 15° . The results are shown in table 2. (See Fig. 28). It is observed that the reduction in torque is more than reduction in thrust.

$N = 4$, pitch angle = 6° .

Sweep angle	C_q / σ	C_t / σ
0°	0.00290	0.0349
2°	0.00235	0.0348
5°	0.00230	0.0342
15°	0.00220	0.0336

Table 2. Effect of tip sweep on Torque and thrust.

Keeping the sweep angle 5° , the performance calculations were carried out for various pitch angles. These results were compared with straight rectangular blade results, as shown in Table 3. Results indicate that there is more reduction in torque in comparison to thrust.

Pitch angle	C_q / σ		C_t / σ	
	Straight blade	5° tip sweep	Straight blade	5° tip sweep
4°	0.0018	0.0016	0.019	0.0187
6°	0.0029	0.0023	0.049	0.0342
8°	0.0046	0.0036	0.053	0.0521
10°	0.0067	0.0042	0.0731	0.0724
12°	0.0092	0.0068	0.0942	0.0932

Table 3. Comparison of swept-tip results with straight blade results.

Figure 29 shows the effect of 5° tip sweep of rotor blade on performance. It is observed that (aft sweep) reduction in rotor power, which has been observed in experimental studies.

Keeping the pitch angle 6° , the effects of tip sweep on bound circulation, effective angle of attack, induced velocity, induced angle of attack and load distribution along the span were calculated. The effect of tip sweep on blade bound circulation is shown in Fig 30. The reduction in bound circulation was observed. Figure 31 shows the effect of tip sweep on the effective angle of attack. The results showed that the reduction in angle of attack as compared to rectangular blade results. The load distribution along the span shown in Fig 32 for various sweep angles. The reduction in lift was found as similar observation was made for fixed swept wing. The variation of induced velocity along the span for various tip sweep angles was shown in Fig 33. The increase in induced velocity was found as comparatively rectangular blade. The induced angle of attack along the span for various tip sweep angles was shown in Fig 34. The results shows, near the blade root the increase in induced angle of attack is more as comparatively tip.

Chapter 5

CONCLUSIONS

In this study, a prescribed wake model has been developed to study the hover performance of a swept tip rotor blade. The model has been used to evaluate the rotor thrust and rotor torque for various values of tip sweep and rotor pitch angles. The important observation of this study is that tip sweep reduces both rotor thrust and rotor torque in comparison to a straight blade. The reduction in torque is observed to be more pronounced than the reduction in thrust. A similar observation has also been made in experimental rotor tests.

Chapter 6

SUGGESTIONS FOR FUTURE WORK

1. In this study, the rectangular swept tip blade was considered. The model can be improved by including taper effect also.
2. Additional aerodynamic phenomena related to compressibility, radial flow and dynamic stall effects may be included to develop a prescribed wake model applicable for forward flight.

APPENDIX A

*Combined Momentum / Blade element Equations
(used for non-uniform inflow calculation) (Ref. 31)*

$$\lambda_i = -\left(\frac{\lambda_c}{2} + \frac{\sigma a}{16}\right) + \sqrt{\left[\left(\frac{\lambda_c}{2} + \frac{\sigma a}{16}\right)^2 + \frac{\sigma a}{8}(\theta \bar{r} - \lambda_c)\right]}$$

$$\lambda = \frac{V_\infty + v_z}{\Omega R} \quad \lambda_i = \frac{v_z}{\Omega R} \quad \lambda_c = \frac{V_\infty}{\Omega R}$$

$$dC_T = \frac{\sigma a}{2}(\theta \bar{r}^2 - \lambda \bar{r})d\bar{r}$$

where

V_∞ axial velocity

v_z induced velocity

Ω angular velocity of rotor

σ solidity ratio

θ total angle of attack at the section

a lift curve slope

R radius of the rotor blade

C_T coefficient of thrust

APPENDIX B

Simpson's Rule of Integration (Ref. 32)

Algorithm

This algorithm computes the integral $J = \int_a^b f(x) dx$ from given values

$f_j = f(x_j)$ at equidistant $x_0 = a$, $x_1 = x_0 + h$, $x_{2m} = x_0 + 2mh = b$ by

Simpson's rule where $h = (b-a)/2m$

INPUT : $a, b, m, f_0, \dots, f_{2m}$
OUTPUT : approximate value \tilde{J} of J
Compute $S_0 = f_0 + f_{2m}$
 $S_1 = f_1 + f_3 + \dots + f_{2m-1}$
 $S_2 = f_2 + f_4 + \dots + f_{2m-2}$
 $h = (b-a)/2m$
 $\tilde{J} = h/3(S_0 + 4S_1 + 2S_2)$
OUTPUT \tilde{J} Stop
End SIMPSON

Adaptive Integration

Here, the step h is adapted to the variability of $f(x)$: small h , where the variability of $f(x)$ is large and large h where it is small. Changing h is done systematically, usually by halving h , depending on the size of the estimated error over a subinterval. The subinterval is halved if the corresponding error is still too large, that is, larger than a given tolerance (maximum admissible absolute error) or is not halved if the error is less than the tolerance.

REFERENCES

1. Bousman, W.G., "Putting the Aero Back Into Aeroelasticity", Eighth Annual ARO Workshop on Aeroelasticity of Rotorcraft Systems, University Park, PA, October 18-20, 1999.
2. Sadler, G.S., "Development And Application Of a Method For Predicting Rotor Free Wake Positions And Resulting Rotor Blade Airloads," NASA CR-1911, Dec. 1971.
3. Bagai, A., and Leishman, J.G., "Challenges in Understanding the Vortex Dynamics of Helicopter Rotor Wakes," *AIAA Journal*, Vol. 36, No. 7, July 1998, pp. 1130-1140.
4. Landgrebe, A.J., "The Wake Geometry of a Hovering Helicopter Rotor and Its Influence on Rotor Performance," *Journal of the American Helicopter Society*, Vol. 17, No.4, Oct. 1972, pp. 3-15.
5. Haertig, J., Gnemmi, P., Johe, Ch., "*Hovering Rotor Performance: A Panel hod Coupled with a Navier-Stokes Method*",
6. Bramwell, A.R.S., *Helicopter Dynamics*, Edward Arnold, London, 1976.
7. Kocurek, J.D., and, Tangler, J.L., "A Prescribed Wake Lifting Surface Hover Performance Analysis," *Journal of the American Helicopter Society*, Vol. 22, No.1, Jan. 1977, pp. 24-35.
8. Caradonna, F., Hendley, E., Silva, M., Huang, S., Komerath, N., Reddy, U., Mahalingam, R., Funk, R., Wong, O., Ames, R., Darden, L., Villareal, L., and Gregory, J., "An Experimental Study of Rotor in Axial Flight," *Journal of the American Helicopter Society*, Vol. 4, No. 2, Apr. 1999, pp. 101-108.
9. Jain, R., Conlisk, A. T., "Interaction of Tip-Vortices in the Wake of a Two-Bladed Rotor in Axial Flight," *Journal of the American Helicopter Society*, Vol. 45, No. 3, July 2000, pp. 157-164.
10. F.Techen-Fo et al, "Improved Vortex Ring Model For Helicopter Pitch up Prediction", 23rd European Rotorcraft Forum 16-18 September 1997, Germany.

11. J.Gordon Leishmen, "*Principles of Helicopter Aerodynamics*", Cambridge University press 2000.
12. Mc Veigh, M.A. and Mc Hugh, F.J. "Recent Advances in Rotor Technology at Boeing Vertol", 38th annual forum of the American Helicopter Soc., Anaheim, CA, May 4-7.
13. Jing G.Yen, "*Effects of Tip Shape on Dynamics, Cost, Weight, Aerodynamic Performance, and Aeroelastic Response*", Journal of the American Helicopter Society, Oct.1994, 37-45.
14. Thomas H.Maier, "*Analytical Model Sensitivity Study for Aeroelastic Stability of Straight and Swept-Tip Rotor Blades*", Abstract for the 26th European Rotorcraft forum 26-29 September 2000, The Hague, Netherlands.
15. Weller, W.H., "*Experimental Investigation of Effects of Blade Tip Geometry on Loads and Performance for an Articulated Rotor System*", AVRAD-COM TR 78-53, Jan 1979.
16. Desopper, A., Lafon, P., Philippe, J.J., and Prieur, J., "*Effect of an Anhedral Sweptback Tip on the Performance of a Helicopter Rotor*", 13th European Rotor Craft Forum, Arles, France, Sep 1987.
17. Stroub, R.H., Rabbott, J.P., Jr., and Niebanck, C.F., "*Rotor Blade Tip Shape Effects on Performance and Control Loads From Full- Scale Wind Tunnel Testing*", Journal of the American Helicopter Society, Vol 24,(5), Oct 1979.
18. Bagai, A. and Leishman, J.G., "Rotor Free-Wake Modeling Using a Psuedo-Implicit Relaxation Algorithm," *Journal of Aircraft*, 32, (6), Nov-Dec 1995, pp. 1276-1285.
19. Johnson, W., "Recent Developments in Rotary-Wing Aerodynamic Theory," *AIAA Journal*, Vol. 24, No.8, Aug. 1986, pp. 1219-1244.
20. Johnson, W., "*Airloads And Wake Models For a Comprehensive Helicopter Analysis*," *Vertica*, Vo. 14, No.3, 1990, pp. 255-300.
21. Johnson, W., "Development Of a Comprehensive Analysis For Rotorcraft-I. Rotor Model And Wake Analysis," *Vertica*, Vol. 5, 1981, pp. 99-129.
22. Baskin, V.E., Vil'dgrube, L.S., Vozhdayev, E.S., and Maykapar, G.I., *Theory of the Lifting Airscrew*. NASA-TT F-823, Feb. 1976ns, Inc., New York., 1984.

23. Stepniewsky, W.Z., and Keys, C.N. *Rotary-Wing Aerodynamics*.
Dover Publications, Inc., New York., 1984.
24. Srinivasan, G.R., Baedar, J.D., Obayashi, S., and McCroskey, W.J., "Flowfield of a Lifting Rotor in Hover: A Navier-Stokes Simulation," *AIAA Journal*, Vol. 30, No. 10, 1992, pp. 2371-2378.
25. Berkman, M.E., and Sankar, L.N., "Navier-Stokes/Full-Potential/Free-Wake Method for Rotor Flow," *Journal of Aircraft*, Vol. 34, No. 5, 1997, pp. 635-640.
26. Landgrebe, A.J., Moffitt, R.C., and Clark, D.R., "Aerodynamic Technology for Advanced Rotorcraft-Part I," *Journal of The American Helicopter Society*, Vol. 22, No. 2, April 1977, pp. 21-27.
27. Abbot, I.H., and Doenhoff, A.E.V., *Theory of wing sections*, Dover Publications, Inc., New York, 1959.
28. Cho, M.H., Jeon, S.M., Woo, S.H., and Lee, I., "Refined Aeroelastic Analysis of Hingeless Rotor Blades in Hover," *Journal of Aircraft*, Vol. 34, No. 3, May-June 1997, pp. 408-415.
29. Rohin Kumar, M., "Performance Prediction of Helicopter Rotor in Hover and Axial Flight Using Prescribed Bake Model", M.Tech Thesis, IIT Kanpur, March 2001.
30. McCormick, B.W., *Aerodynamics, Aeronautics, And Flight Mechanics*, John Wiley & Sons, Inc., 1995, pp.110.
31. Johnson, W., *Helicopter theory*, Princeton University Press, Princeton, NJ, 1980.
32. Berton, E., Favier, D., and Maresca, C., "Hover Performance Prediction Using Full-Potential Method and Comparison with Experiments", *Journal of Aircraft*, Vol. 37, No. 5, Sept.-Oct. 2000, pp. 803-809.

FIGURES

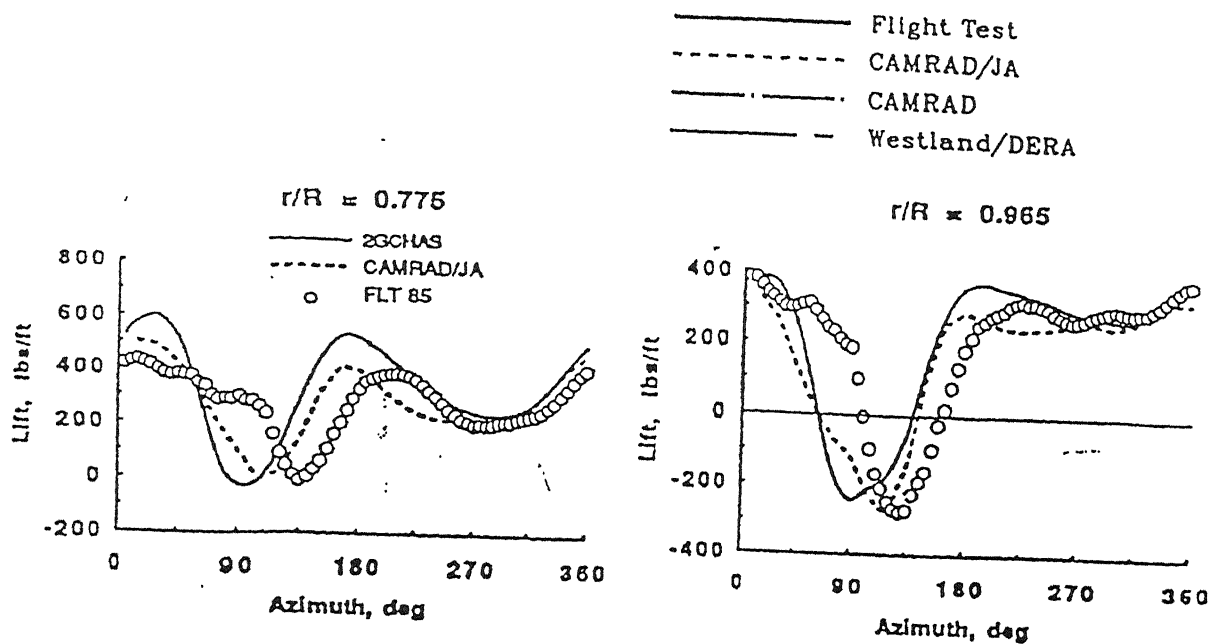


Fig. 1. Airloads Estimations for Two Radial Stations (Ref.1)

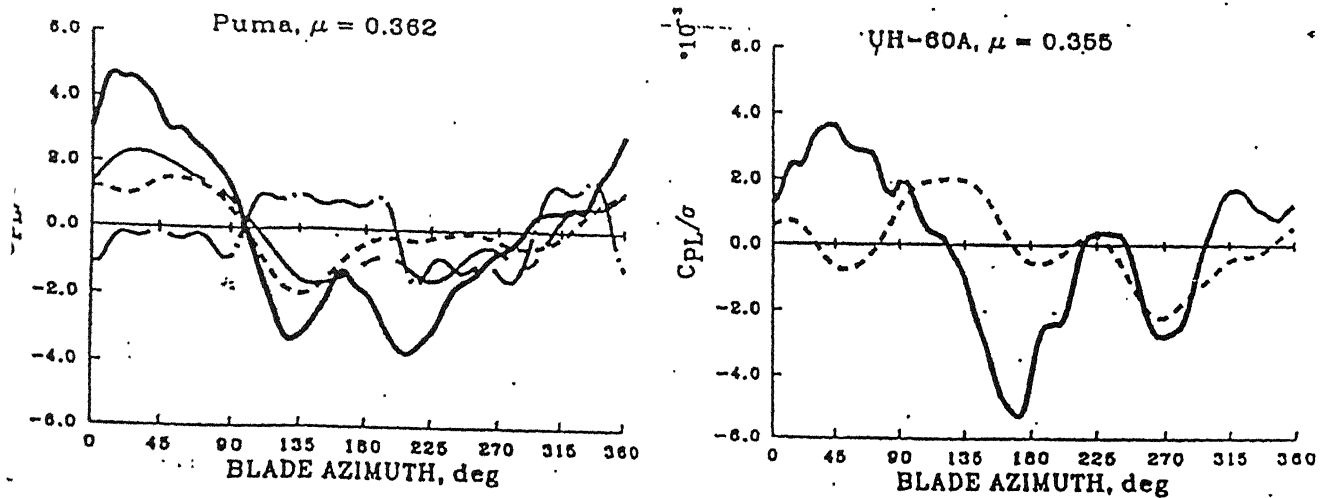


Fig. 2. Oscillatory Pitch -Link Loads Estimation (Ref. 1)

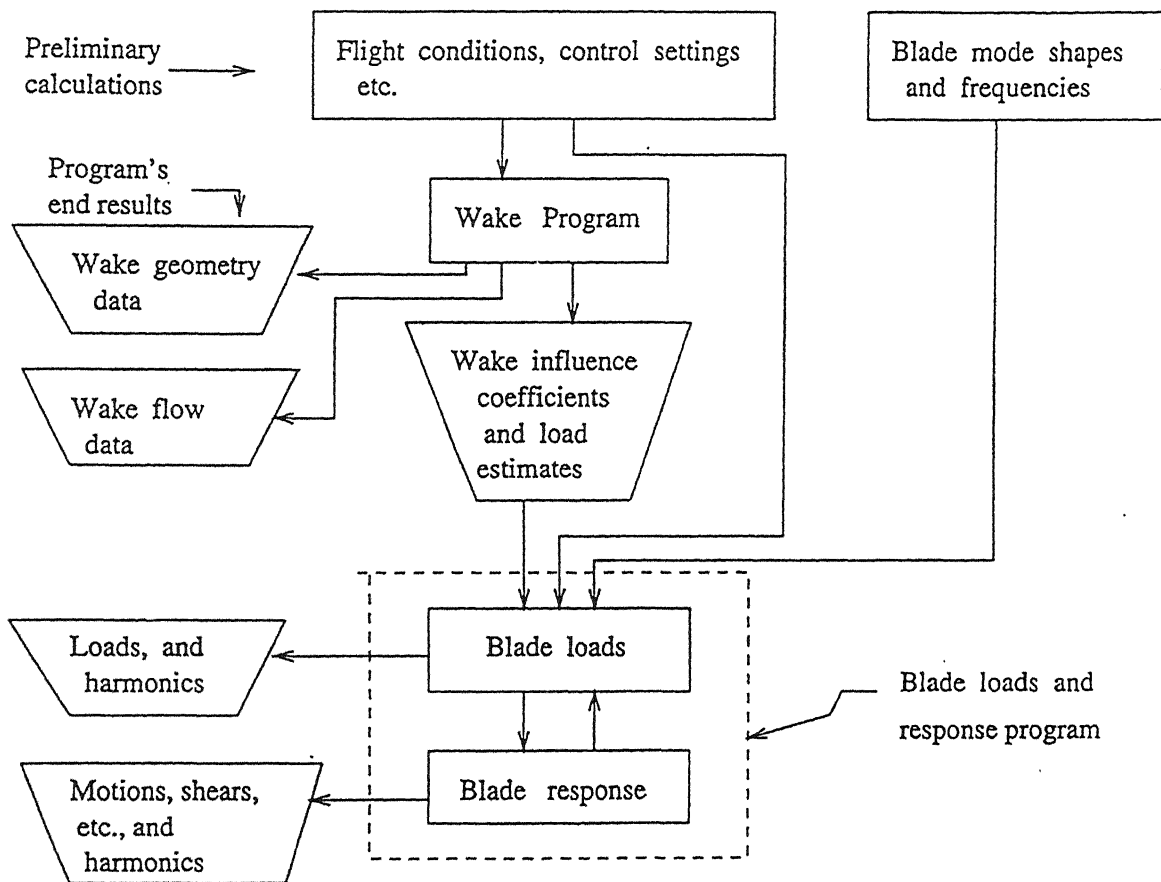


Fig. 3. Flowchart of Sadler's Model (Ref. 2)

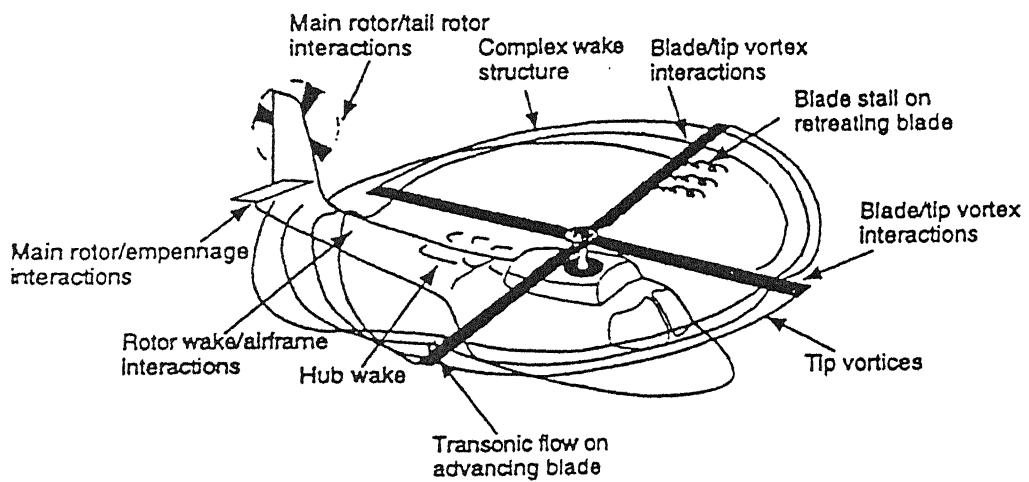


Fig. 4. Flow Field of a Helicopter in Forward Flight (Ref.3)

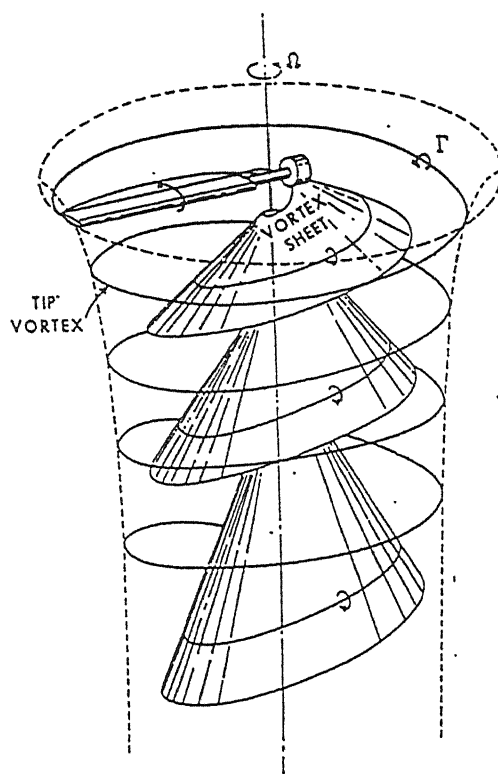


Fig. 5. Gray's Schematic of Hovering Wake Structure (Ref. 4)

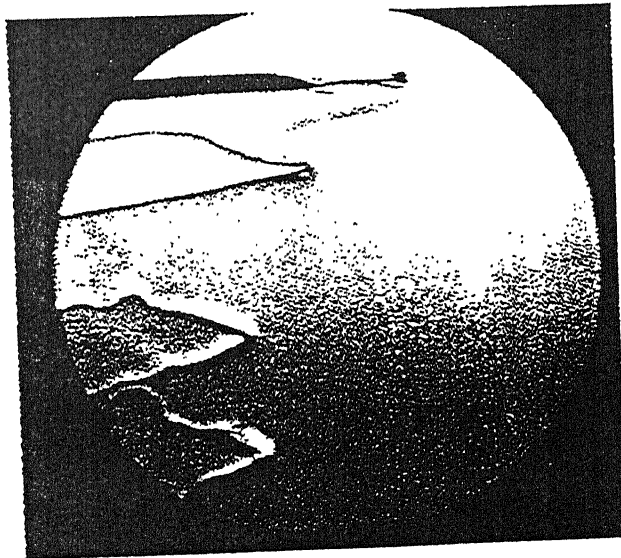


Fig. 6. Visualization of Tip Vortex Shed (Ref.5)

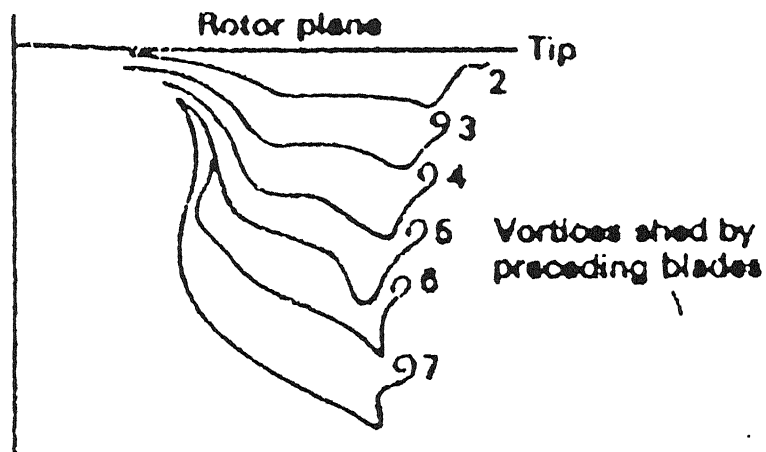


Fig. 7. Vortex Wake Calculated from Free-Wake Analysis (Ref.6)

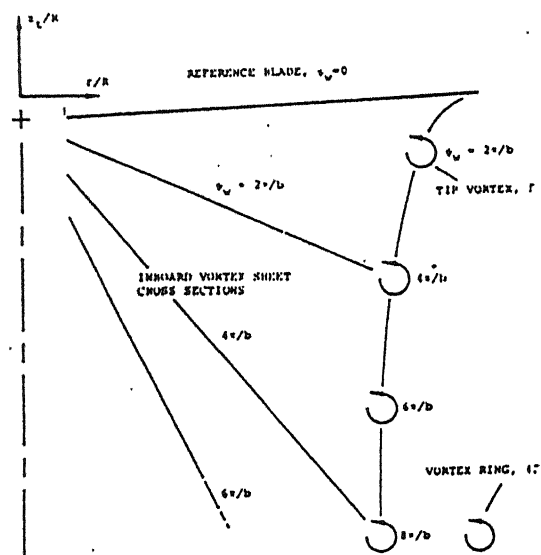


Fig. 8. Cross-Section of Wake With Vortex-Ring (Ref.7)

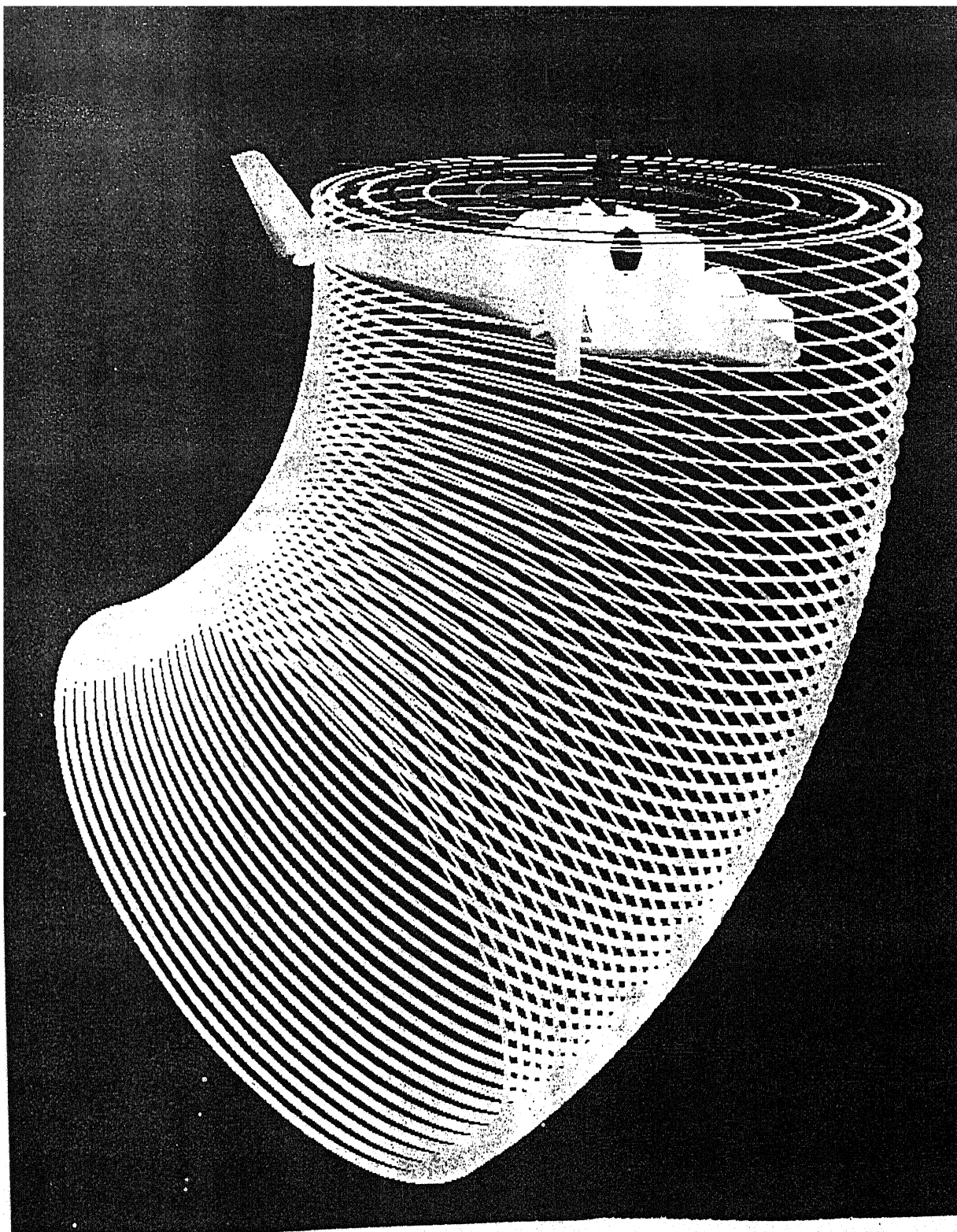


Fig. 9. Vortex Rings Model (Ref.10)

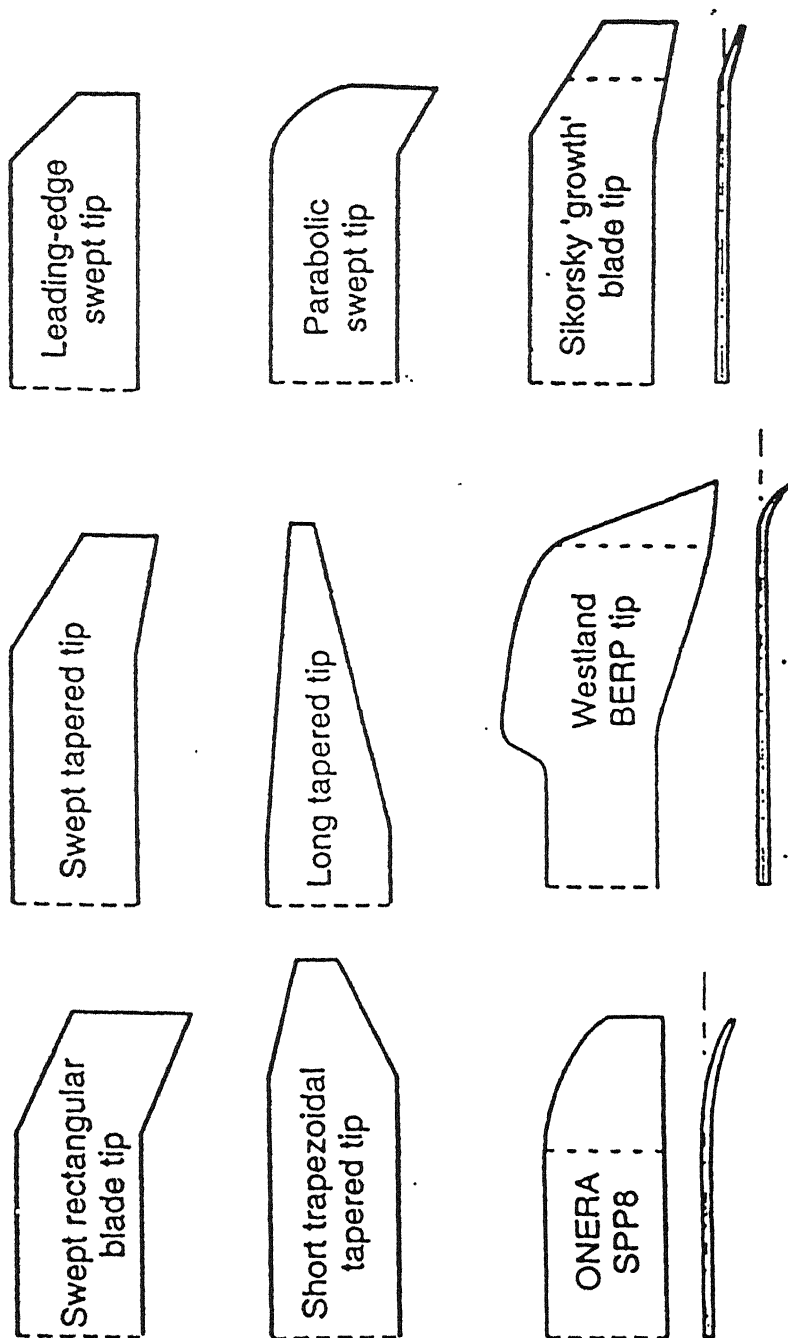


Fig.10.Blade Tip Shapes (Ref.11)

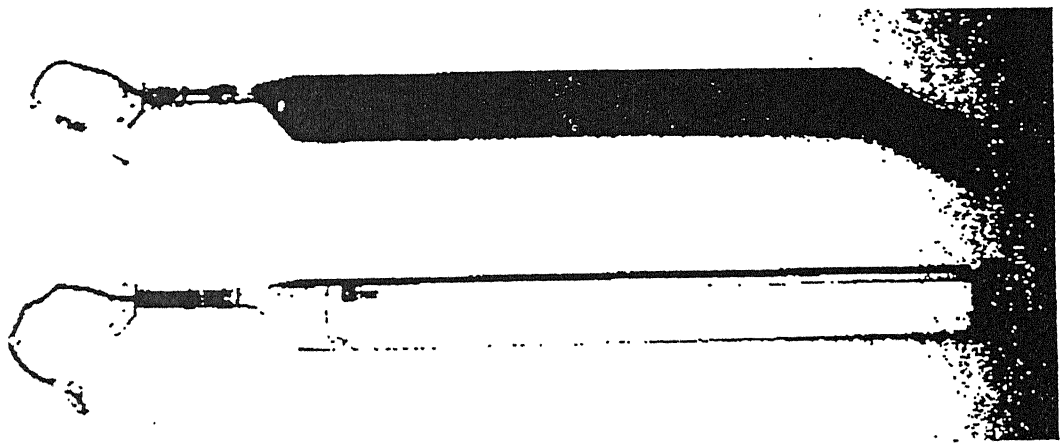


Fig. 11. Planform View of Straight and Swept-Tip Blades (Ref.14)

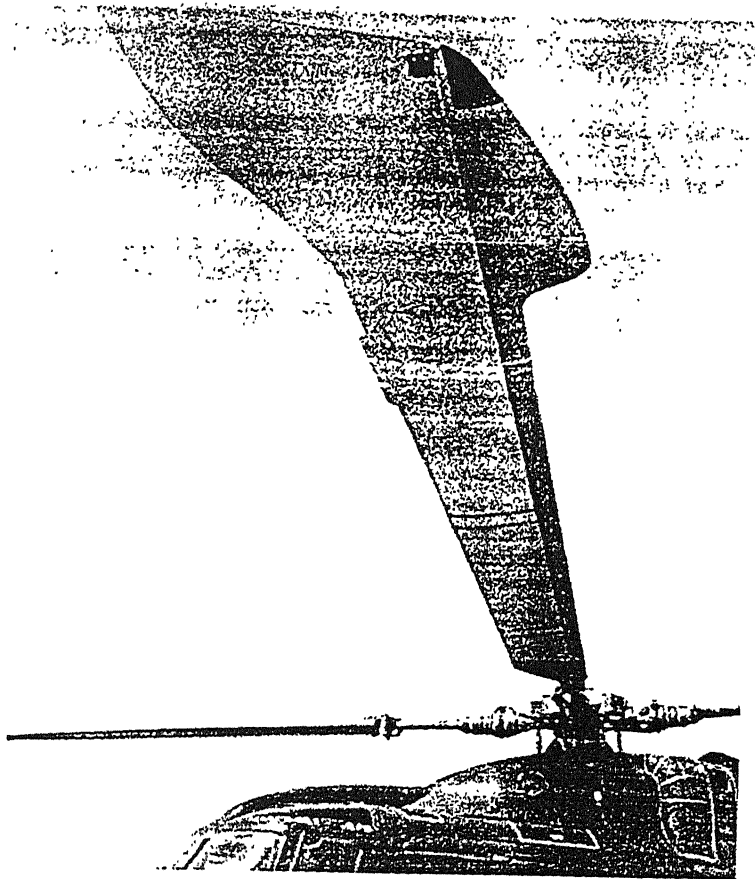


Figure. 12. BERP Rotor Blade (Ref.11)

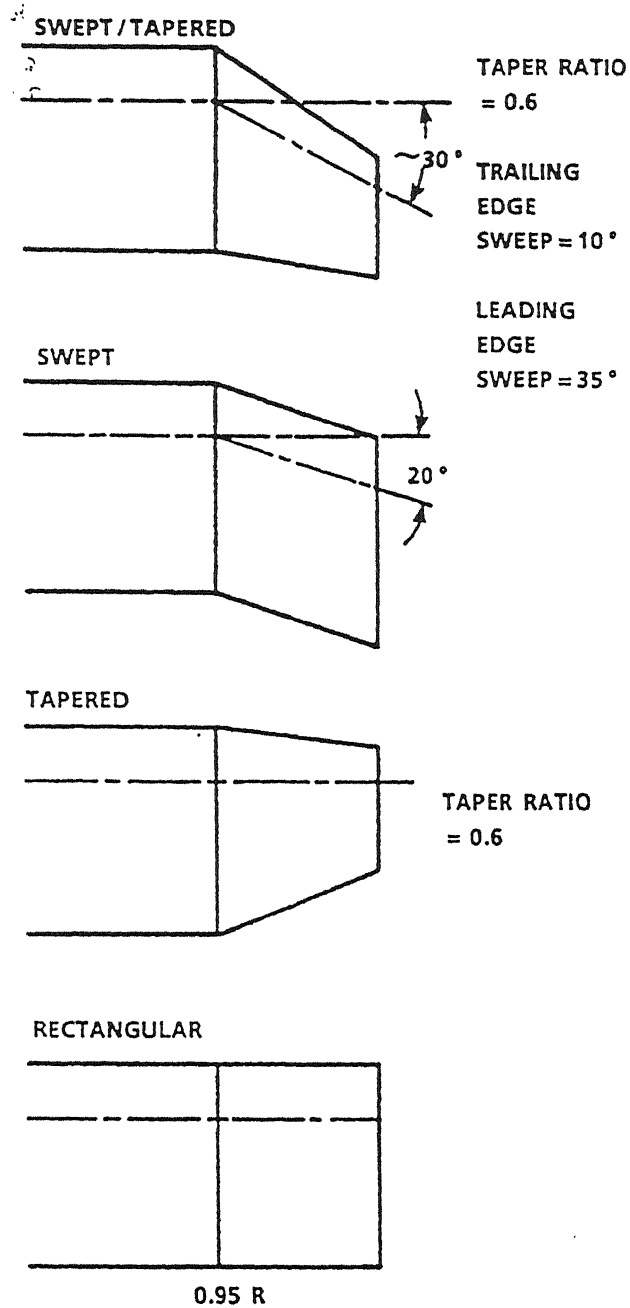


Fig. 13. Tip planform geometry (Ref.13)

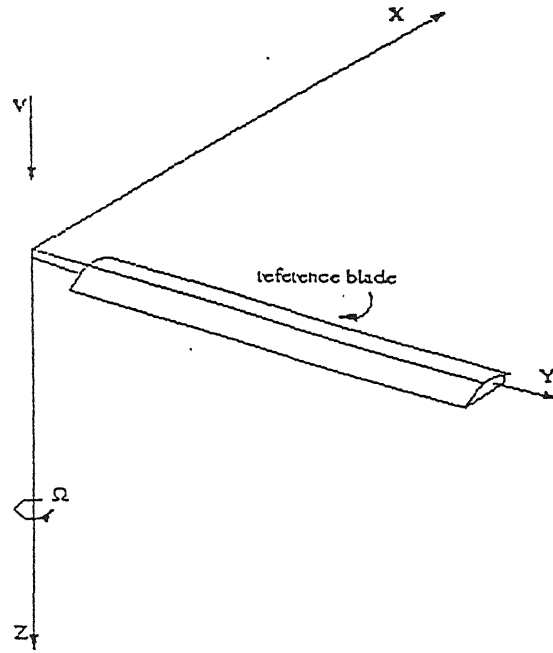


Fig. 14. Rotor Coordinate System.

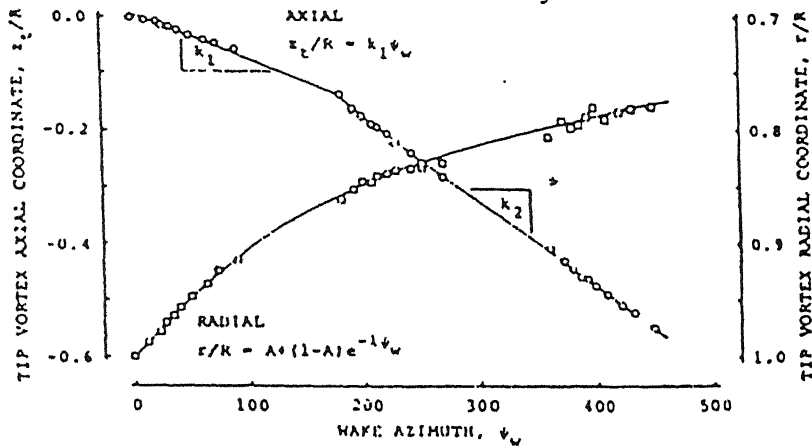


Fig. 15a. Tip Vortex Trajectory. (Ref.5).

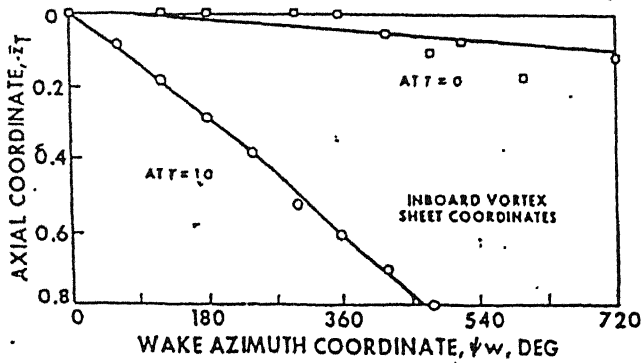


Fig 15b. Inboard Vortex Sheet Coordinates. (Ref.4).

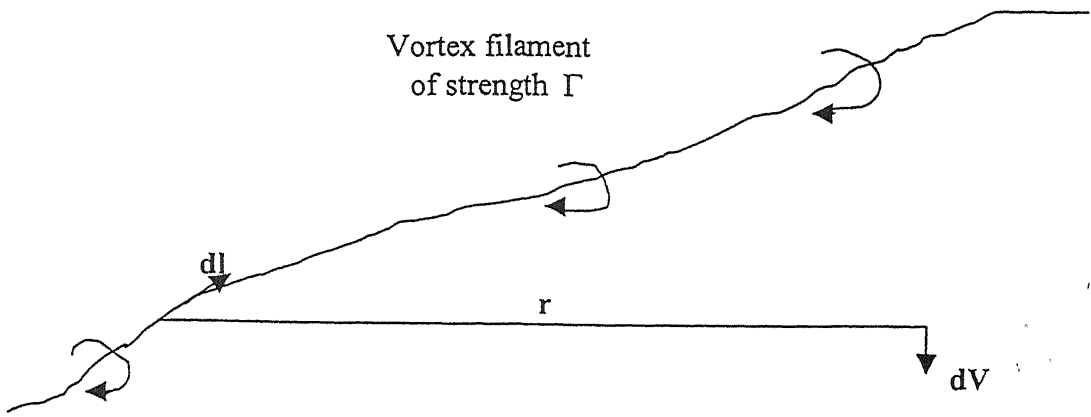


Fig .16. Biot-Savart Law Definition

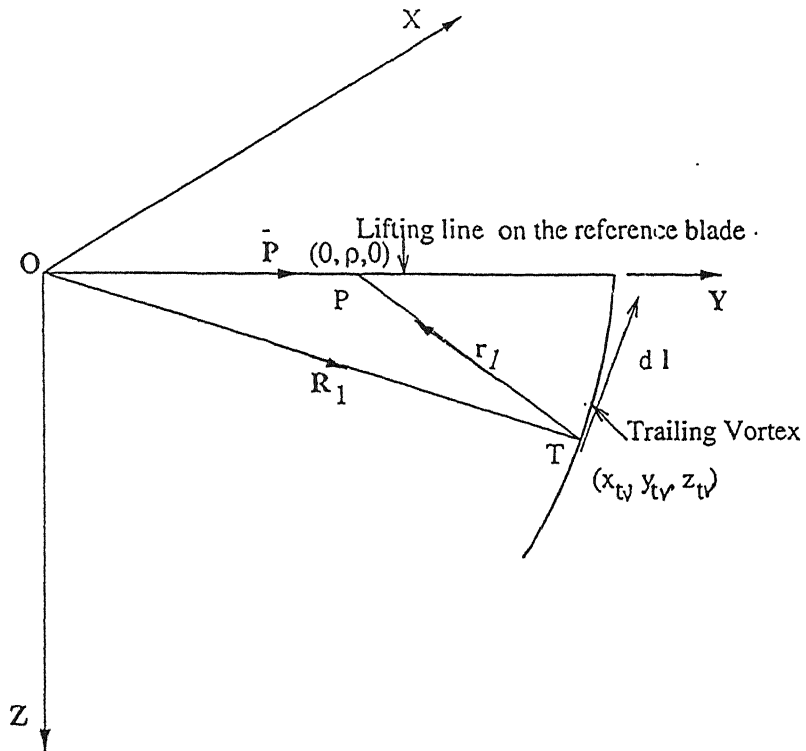


Fig .17. Diagram Showing the Trailing Vortex

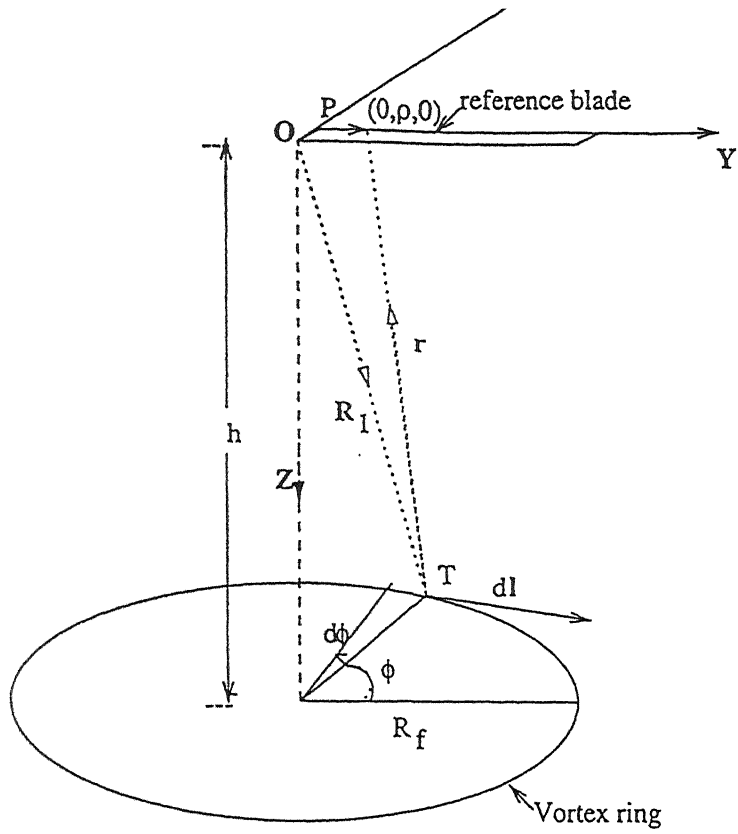


Fig.18. diagram showing the position of the vortex ring.

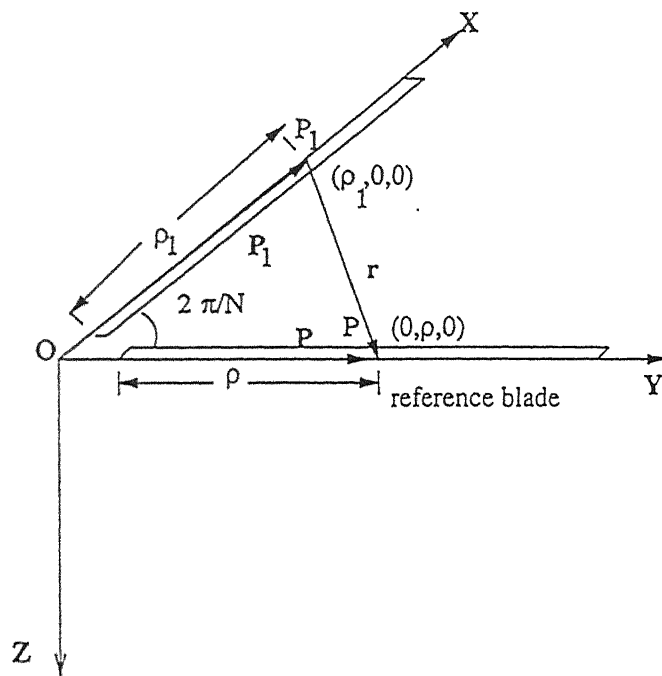


Fig .19. Diagram Showing the Bound Vortex Effect

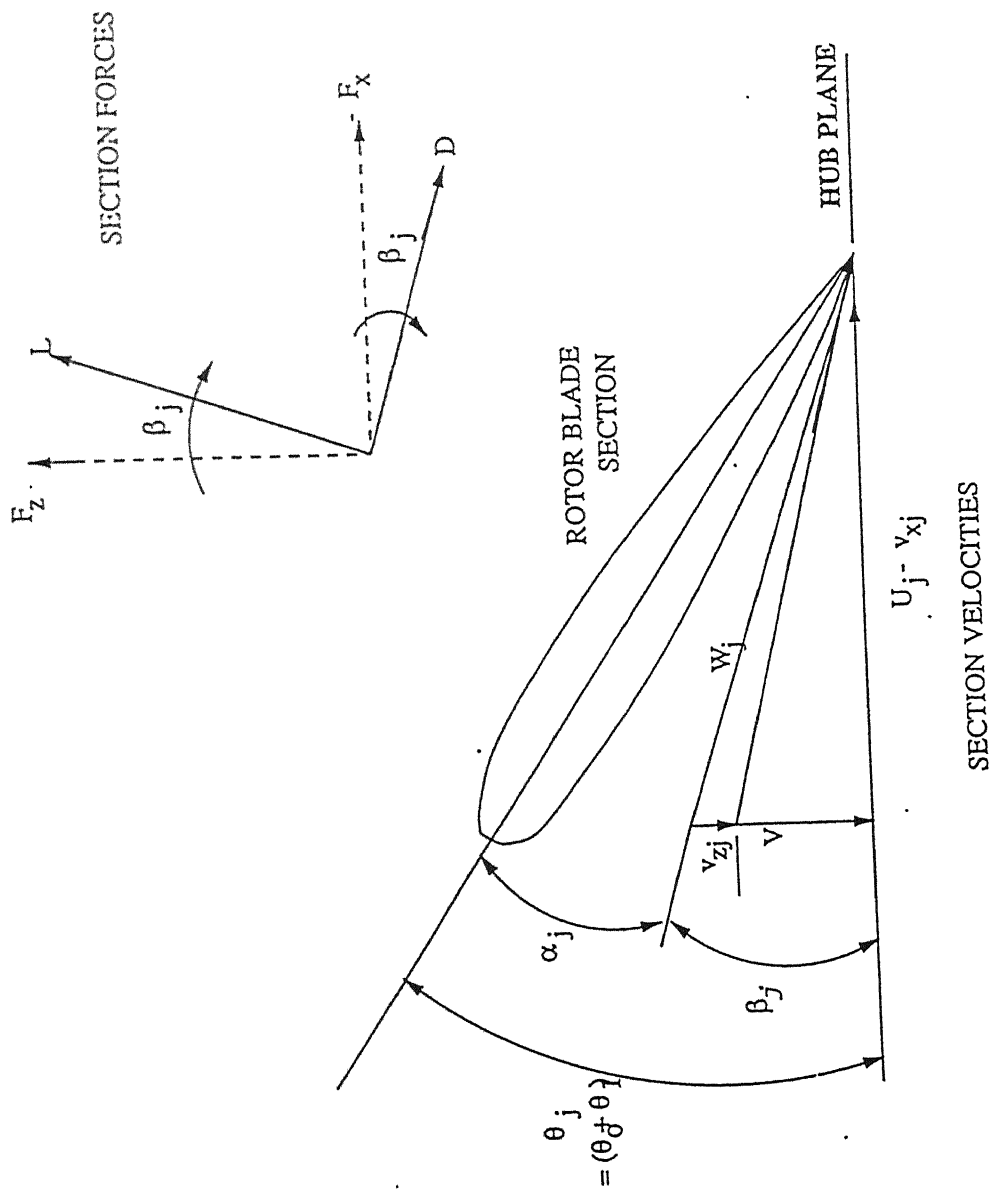


Fig.20. Flow at a Blade Section.

.a, b, c,.....y, z : control points at three-quarter chord

1, 2, 3,.....n, n+1 : trailing vortices from bound vortex located at quarter chord

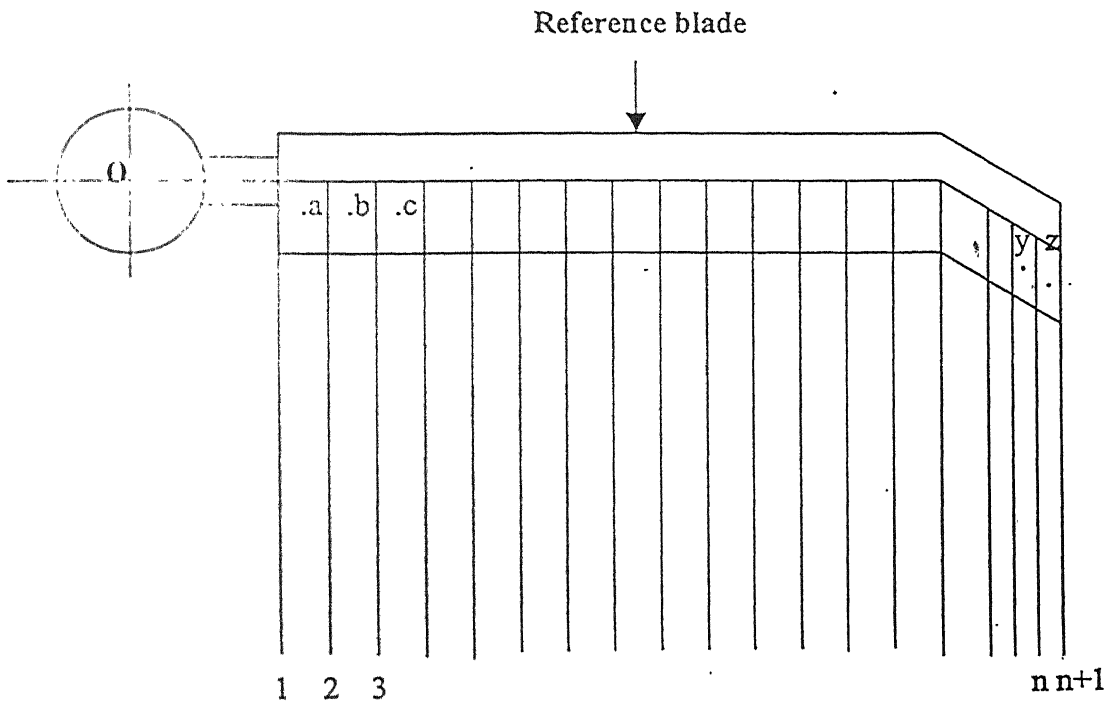


Fig. 21. Trailing Vortices From the Swept-Tip Rotor Blade

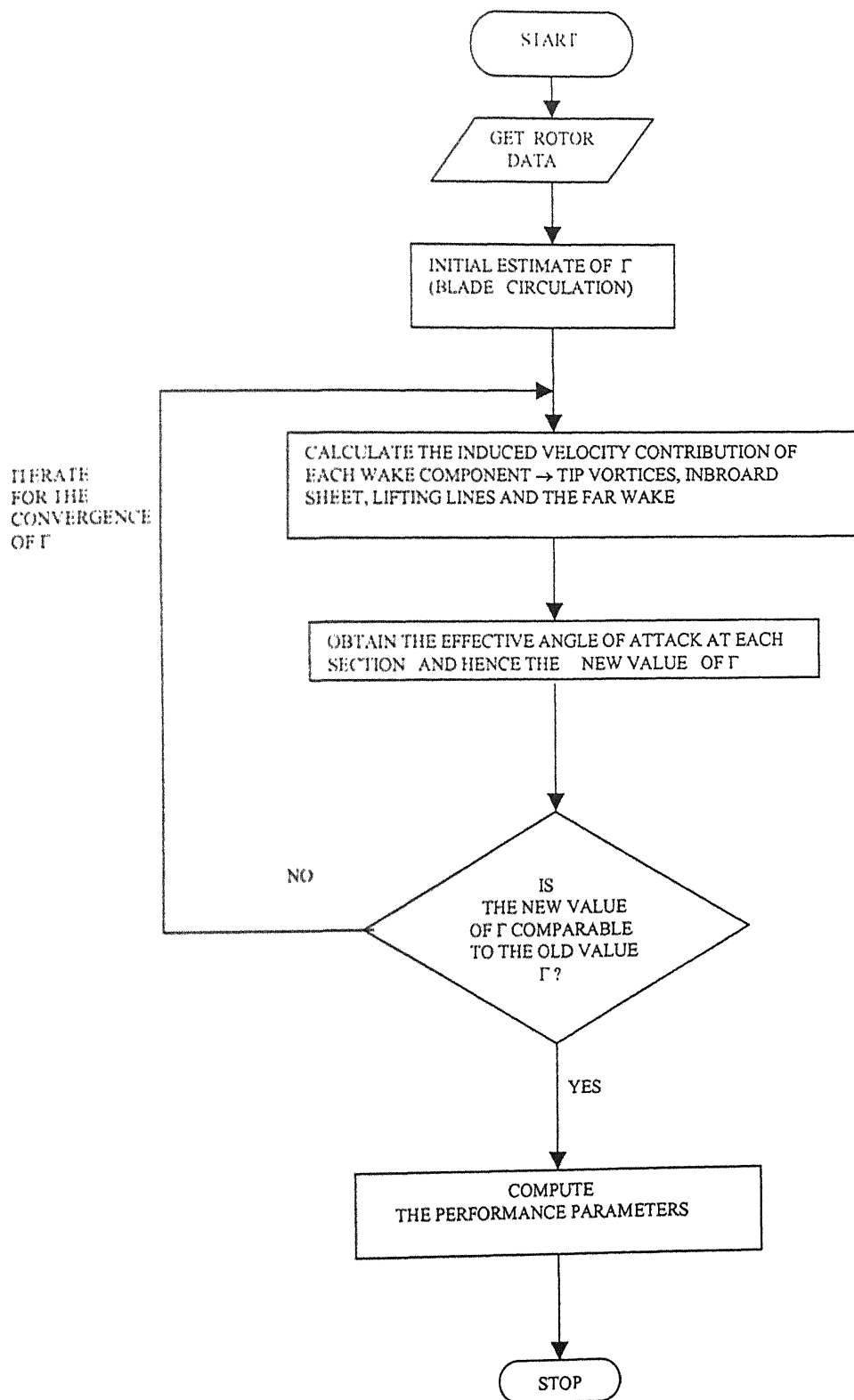


Fig. 22. Flow Chart of the Program

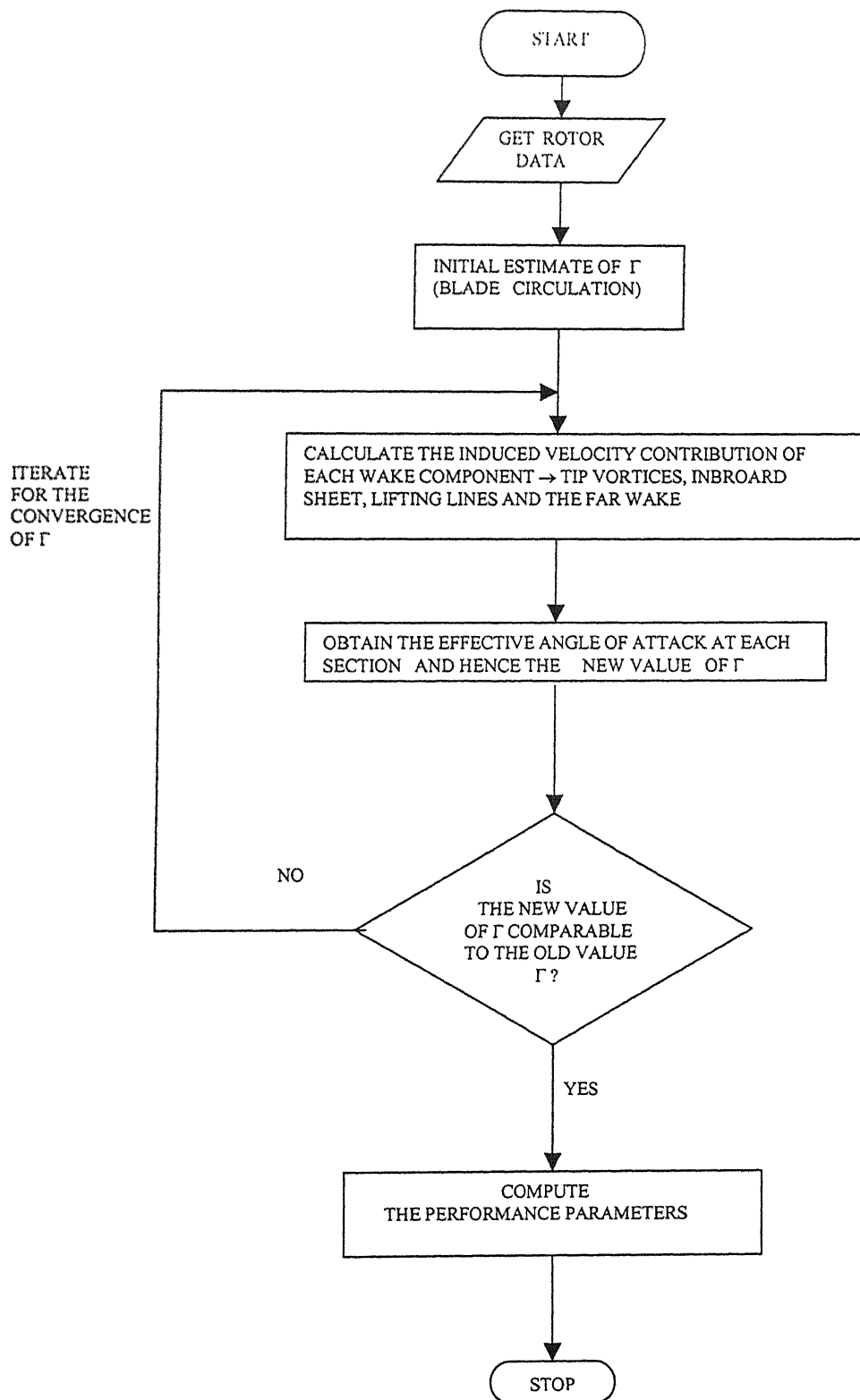


Fig. 22. Flow Chart of the Program

Wake from one of the blades of a two-bladed rotor in hover
(pitch = 4 deg.)

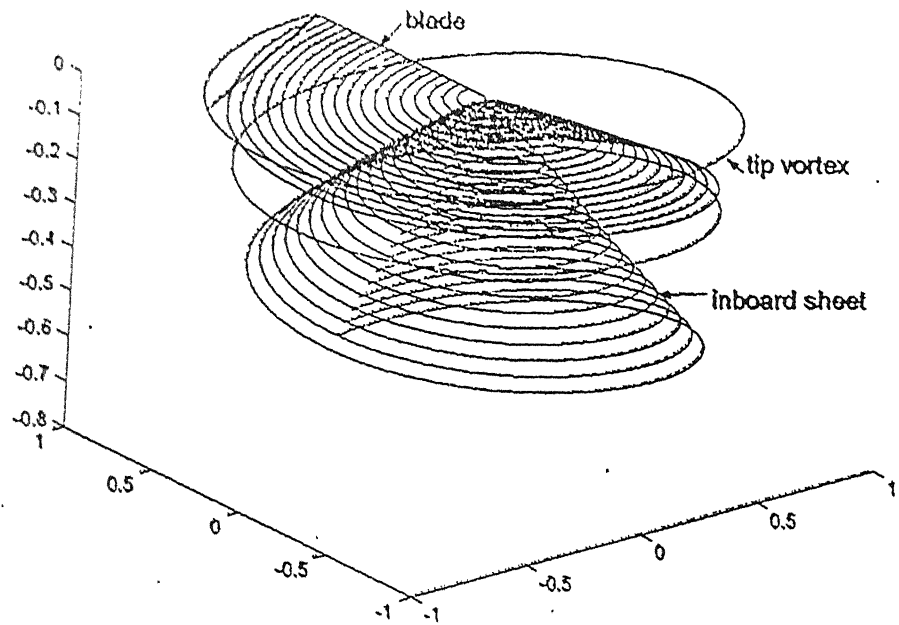


Fig 23a. Wake Constructed Using Empirical Equations

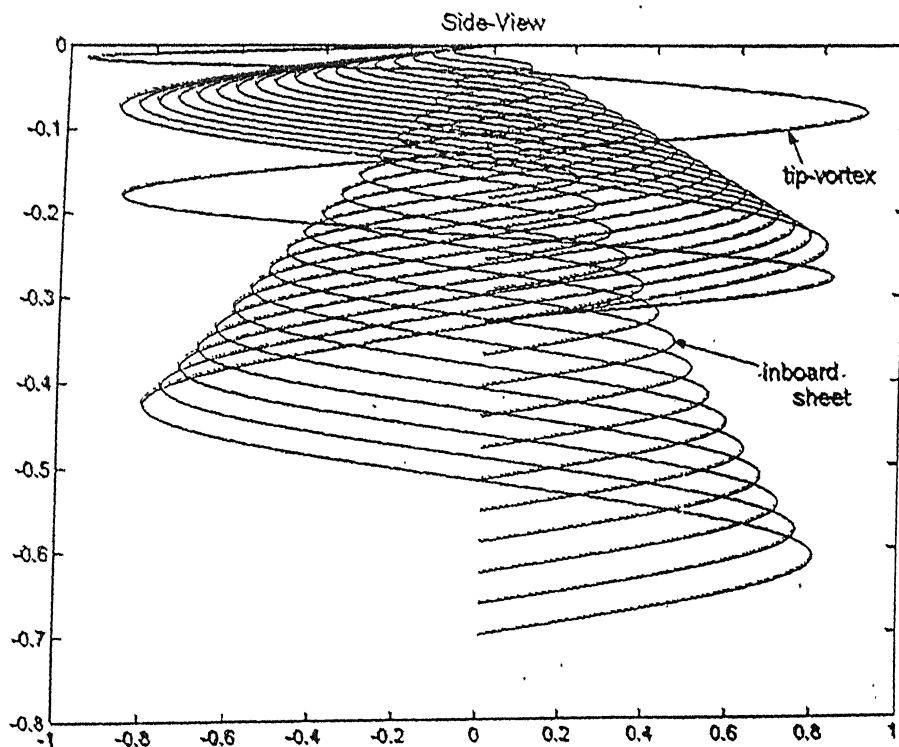


Fig 23b. Side view of the Wake

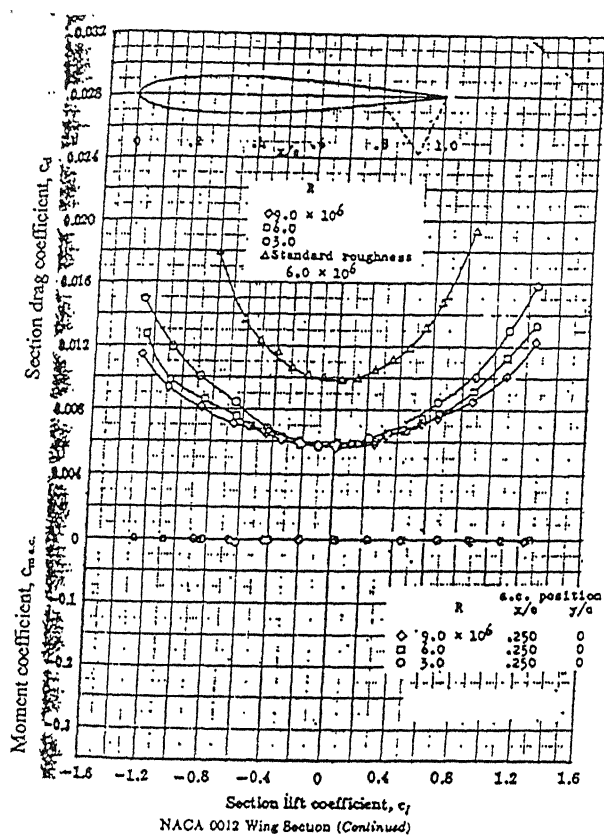
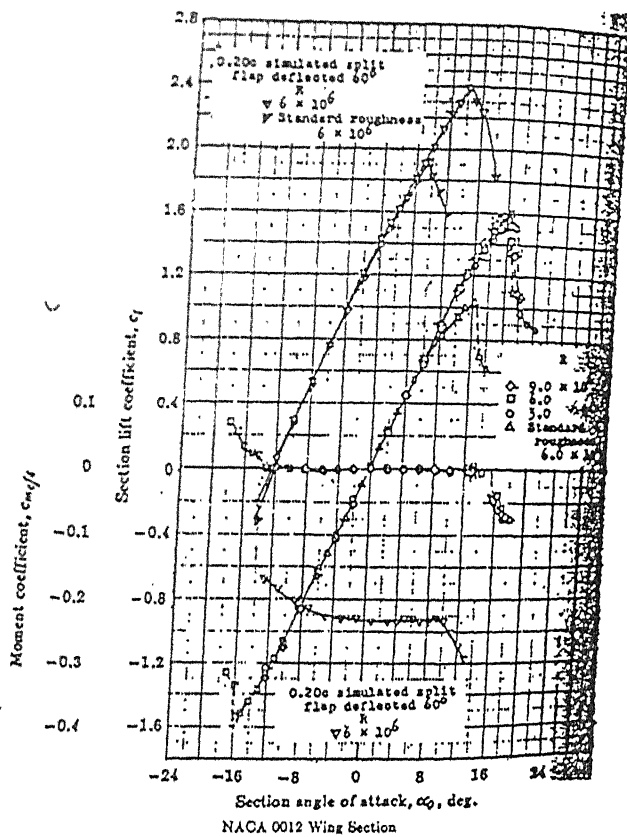


Fig 24. NACA 0012 Curves

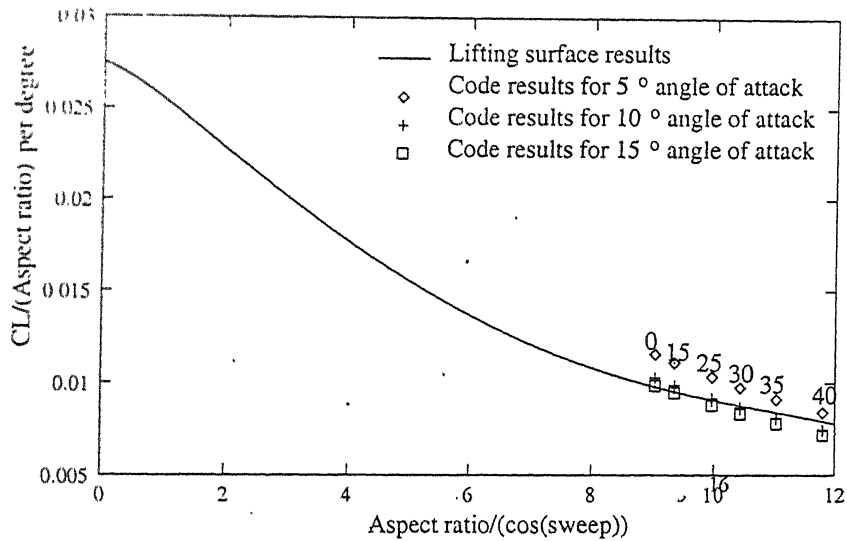


Fig. 25 Finite wing validation (The numbers by the symbols represent sweep angles in degrees)

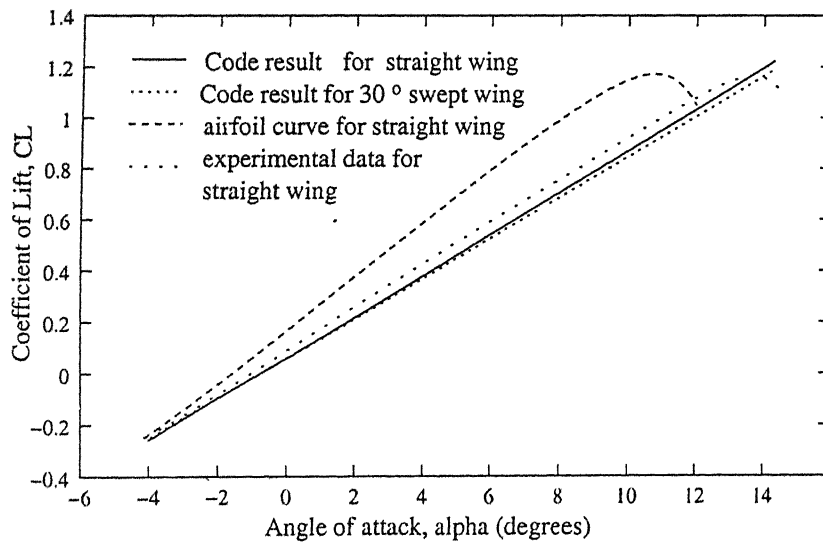


Fig 26. Effect of sweep on fixed wing lift

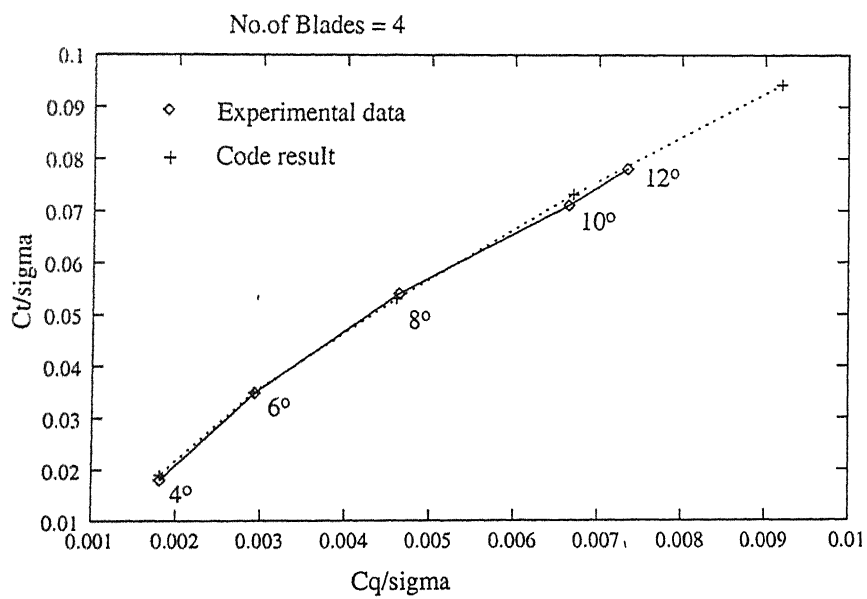


Fig 27. Performance curve for rectangular blades
(The numbers by the symbols represent pitch angles in degrees)

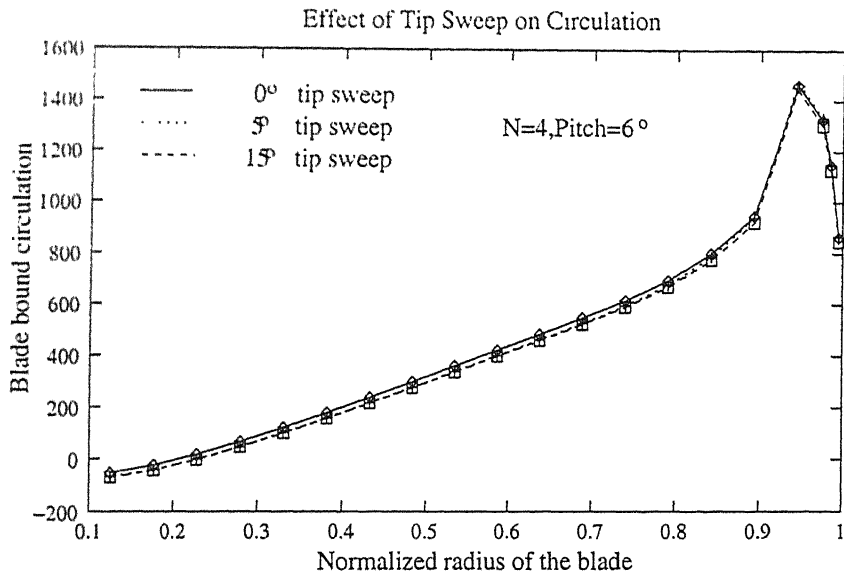


Fig 30. Variation of bound circulation along radius

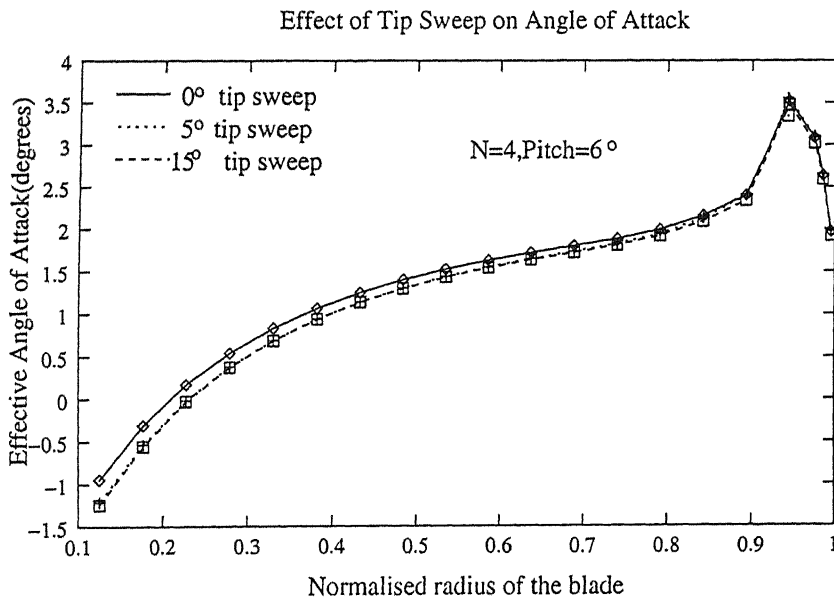


Fig 31. Variation of effective angle-of-attack with radius

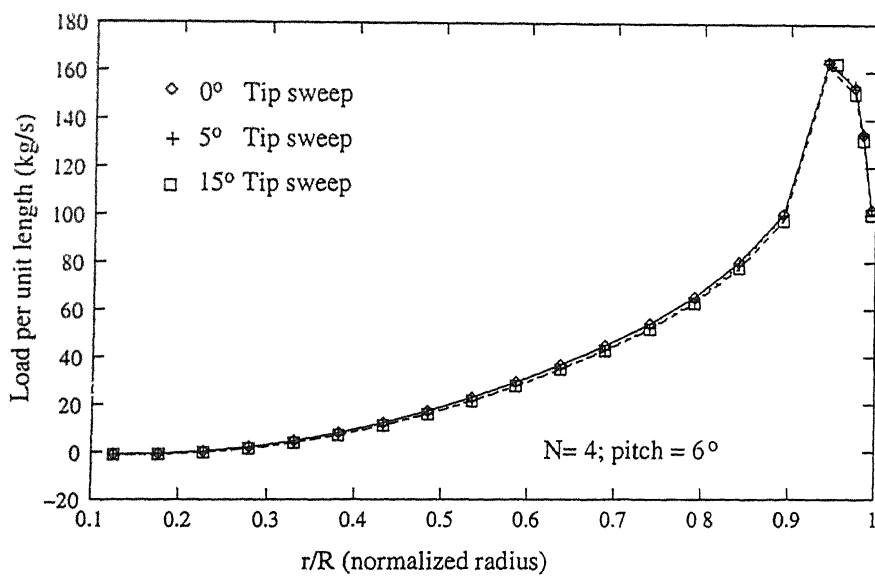


Fig 32. Variation of Load along the span

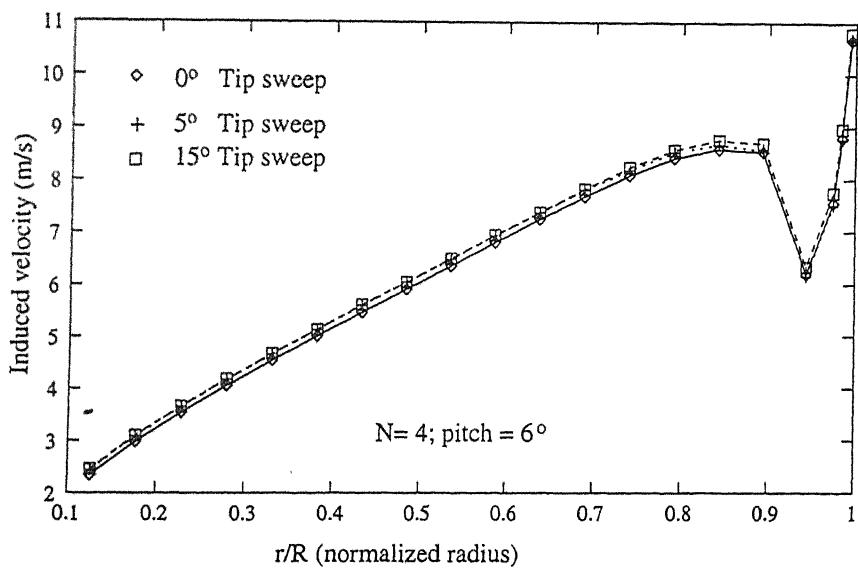


Fig 33. Variation of vertical induced velocity along radius

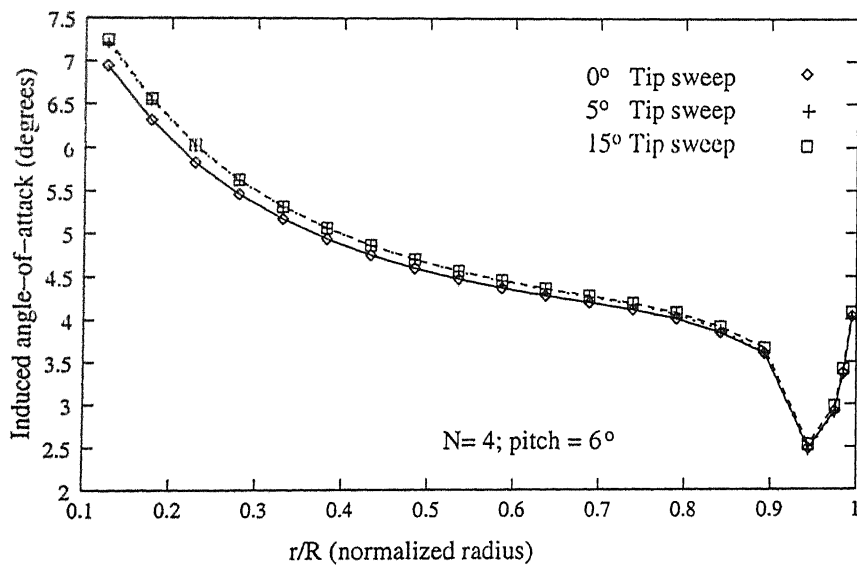


Fig 34. Variation of Induced angle-of-attack along radius

"Verification for a fixed wing

"C language program is used

Definition of Variables used

a : lift curve coefficient
avC : chord
Ar : area of the wing
Croot : root chord
Ctip : tip chord
CL : coefficient of lift
gamma : circulation of the vortices
gammal : circulation of lifting line
gammaln : new circulation value of lifting line
N : number of control points
rcp : locations of control points
rho : density
rA : stations on the wing
sweep : sweep angle
S : span
theta0 : angle of attack
theta1 : twist rate
u : speed of plane m/s
v : induced velocity

```
#include<stdio.h>
#include<math.h>
main()
{
    int i,j,jj,N,flag,flag1;
    float a,avC,Croot,Ctip,rho,S,theta1,u,Ar,f1,f2,f3,L;
    float C[20],rA[20],rcp[20],theta0[40],v[20],CL[40],gamma[20],
        gammal[20],gammaln[20],sweep;

    printf("Enter the value of lift curve slope\n");
    scanf("%f",&a);
    printf("Enter the value of average chord\n");
    scanf("%f",&avC);
    printf("Enter the value of root chord\n");
    scanf("%f",&Croot);
    printf("Enter the value of tip chord\n");
    scanf("%f",&Ctip);
    printf("Enter the number of control points\n");
    scanf("%d",&N);
    printf("Enter the value of density\n");
    scanf("%f",&rho);
```

```

printf("Enter the span n");
scanf("%f",&S);
printf("Enter the rate of twist\n");
scanf("%f",&theta1);
printf("Enter the plane speed in m/s \n");
scanf("%f",&u);
printf(" Enter the sweep angle");
scanf("%f", &sweep);
theta0[1]=-0.07;
for(i=2;i<=33;i++)
{
    theta0[i]=theta0[i-1]+0.01;
}
Ar=S*avC;
for(i=1;i<=N;i++)
{
    rA[i]=S/N*(i-1);
    rcp[i]=rA[i]+S/(2*N);
}
rA[N+1]=S;
for(i=1;i<=5;i++)
{
    C[i]=Croot-(Croot-Ctip)*2/S*(S/2-rcp[i]);
}
for(i=6;i<=10;i++)
{
    C[i]=Croot+(Croot-Ctip)*2/S*(S/2-rcp[i]);
}
for(jj=1;jj<=1;jj++)
{
    for(i=1;i<=N;i++)
    {
        gammal[i]=1;
    }
    gamma[1]=-gammal[1];
    gamma[N+1]=gammal[N];
    for(i=2;i<=N;i++)
    {
        gamma[i]=gammal[i-1]-gammal[i];
    }
    for(i=1;i<=N;i++)
    {
        v[i]=0;
    }
    for(i=1;i<=N;i++)
    {
        for(j=1;j<=N+1;j++)
        {
            v[i]=v[i]+gamma[j]/(4*22/7*cos(sweep)*(rA[j]-rcp[i]));
        }
    }
    flag=1;
    while(flag==1)
    {
        for(i=1;i<=N/2;i++)
        {

```

```

    f1 = v[i];
    f2 = u;
    f3 = sqrt(f1*f1+f2*f2);
    gammaln[i] = a*C[i]*f3/2*(theta0[jj]-theta1*
        (S/2-rcp[i]))-atan(f1/f2)+0.0262;
}
for(i=N/2+1;i<=N;i++)
{
    f1 = v[i];
    f2 = u;
    f3 = sqrt(f1*f1+f2*f2);

    gammaln[i] = a*C[i]*f3/2*(theta0[jj]+theta1*
        (S/2-rcp[i]))-atan(f1/f2)+0.0262;
}
flag1=0;
for(i=1;i<=N;i++)
{
    if(abs(gammaln[i]-gammal[i])>=1.0)
    {
        flag1=1;
    }
    gammal[i]=gammaln[i]+0.1*(gammaln[i]-gammal[i]);
}
gamma[1]=-gammal[1];
gamma[N+1]=gammal[N];
for(i=2;i<=N;i++)
{
    gamma[i]=gammal[i-1]-gammal[i];
}
if(flag1==0)
{
    flag=0;
    break;
}
for(i=1;i<=N;i++)
{
    v[i]=0;
}
for(i=1;i<=N;i++)
{
    for(j=1;j<=N+1;j++)
    {
        v[i]=v[i]+gamma[j]/(4*22/7*cos(sweep)*(rA[j]-rcp[i]));
    }
}
}
for(i=1;i<=N;i++)
{
    L=L+rho*u*cos(sweep)*gammal[i]*S/N;
}
CL[jj]=2*L/(rho*u*u*S*avC);
printf("theta0 = %f\t CL = %f\n", theta0[jj], CL[jj]);
}
}

```

```

% Loads on a helicopter rotor blade using
% a prescribed wake model (MATLAB code)

% Definition of Variables used
% a : lift curve coefficient
% as : angle step size
% A : a constant
% Ar : area of the blade
% C : chord
% CD : coefficient of drag
% CL : coefficient of lift
% CQ : torque coefficient
% CT : Thrust Coefficient
% dCT : differential Thrust Coefficient
% gamma : circulation of the vortices
% gammal: circulation of lifting line
% gamman: new value of gamma
% gammat: total circulation of tip vortex
% k1 : Vortex Settling Rate Parameter 1
% k2 : Vortex Settling Rate Parameter 2
% lc : polynomial fitting lift-curve
% lambda1: Wake Contraction Rate Parameter
% lambda : total inflow ratio
% lambdac: axial inflow ratio
% lambdai: induced inflow ratio
% mu : inverse lift to drag ratio
% N : no. of blades
% novs : no.of vortex stations
% ntv : no. of tip vortices
% omega : angular velocity of blade
% p : polynomial fitting drag-polar
% psib : angle between the blades
% psiw : azimuth angle
% R : radius of a blade
% rl :
% rA : stations on the blade
% rb : non-dimensional radius
% rc : root cut-off
% rcp : locations of control points
% rho : density
% rtlf : root tip loss factor
% Rul : Roll up location of tip vortices
% Rux,Ruy,Ruz : coordinates of the roll up
% location
% sigma : solidity ratio (constant chord)
% sweep: tip sweep angle
% T : Thrust
% Treq : Thrust required
% theta : angle of attack
% theta0 : collective pitch
% theta1 : twist rate (radians per unit length)
% theta1R: total twist (in degrees)
% V : axial velocity
% vh : mean induced velocity in hover
% vx,vy,vz : total induced velocity components
% vxf,vyf,vzf :farwake induced velocity

```

```

%a vx1,vy1,vz1 : inboard vortex induced velocity
%a vx1,vy1,vz1 : lifting line induced velocity components
%a vx1,vy1,vz1 : induced velocity components of tip vortex
%a xl,yl,zl : coordinates of inboard vortices
%a xll,yll,zll :
%a xt,yt,zt : coordinates of tip vortex

```

```

%a Blade assumed to be initially along the Y-axis

```

```

global a as A Ar C CL CD CQ CT f1 f2 f3 gamma gammal
global k1 k2 lc lambda lambdal lambdac
global N ntv novs
global omega p
global psib R rA rc rc rho rtf Rul Rux Ruy Ruz
global sigma sweep
global T theta1 theta0 Treq V vh vx vy vz
global vzt vzi vzf

```

```

fid1 = fopen('bladeegl.m','r');
a = fscanf(fid1,'%f',1);
as = fscanf(fid1,'%f',1);
C = fscanf(fid1,'%f',1);
N = fscanf(fid1,'%f',1);
omega = fscanf(fid1,'%f',1);
rho = fscanf(fid1,'%f',1);
R = fscanf(fid1,'%f',1);
rc = fscanf(fid1,'%f',1);
rtf = fscanf(fid1,'%f',1);
Rul = fscanf(fid1,'%f',1);
V = fscanf(fid1,'%f',1);
theta0 = fscanf(fid1,'%f',1);
theta1 = fscanf(fid1,'%f',1);
sweep = fscanf(fid1,'%f',1);
status = fclose(fid1);

```

```

A = 0.78;
Ar = R*C ;
psib = 2*pi/N;
sigma = N*C/(pi*R);
lambdac = V/(omega*R);
lambda = 0.;
theeta = 0.;
theta1R = 180/pi*theta1*(1-rc)*R;

```

```

CL=0;CD=0;CQ=0;CT=0;f1=0;f2=0;f3=0;k1=0;k2=0;lambdal=0;
Rux=0;Ruy=0;Ruz=0;T=0;vx=0;vy=0;vz=0;

```

```

% Discretize the blade
% vortex stations

```

```

novs = round((rtf-rc)/0.05) + 1;
ntv = round((1-rtf)/0.01);
for i = 1:novs
    rA(i) = (rc + (i-1)*(rtf-rc)/(novs-1))*R;
end

```

```

for i = 1:ntv
    rA(i+novs) = rtf*R + i*(1-rtf)/ntv*R;
end
% control points
for i = 1:(novs-1)
    rcp(i) = rA(i)*(rtf-rc)/(2.*(novs-1))*R;
end
for i = 1:ntv
    rcp(i+novs-1) = rA(i+novs-1)+(1-rtf)/(2.*ntv)*R;
end

% *****
% polynomial fitting lift-curve
x1 = [-0.2793 -0.2443 -0.2094 -0.1745 -0.1396 -0.1047...
      -0.0698 -0.0349 0.0 0.0349 0.0698 0.1047 0.1396...
      0.1745 0.2094 0.2443];
y1 = [-1.6 -1.45 -1.3 -1.1 -0.85 -0.625 -0.4 -0.2 0.0...
      0.225 0.4 0.625 0.8 0.925 1.0 0.6];
lc = spline(x1,y1);

% polynomial fitting of drag-polar
x = [-0.8 -0.6 -0.5 -0.4 -0.3 -0.2 -0.1 0.0...
     0.1 0.2 0.3 0.4 0.5 0.6 0.8];
y = [0.018 0.0134 0.0121 0.0112 0.0106 0.0102 0.0099 ...
     0.0098 0.01 0.0102 0.0108 0.0114 0.0124 0.014 0.018];
p = spline(x,y);
% *****

[gamma,gammal] = inigam(1); % initialisation of circulations
[CT] = ThrCoe(theta0);
vh = 1.0;
[vx,vy,vz]=TotInd(1);
[gamma] = Compgam(1);
[CT,CQ,alpha] = PerCal(1);

% Plots of Performance calculations
plot(CT,CQ)
figure(2)
plot(CT/sigma,CQ/sigma)
figure(3)
plot(rcp/R,alpha)
figure(4)
plot(rcp/R,gammal)

%*****End of main program*****

% function for initialization of the blade bound circulation(gammal) values

function[gamma,gammal] = inigam(cc)
global a as A Ar C CL CD CQ CT f1 f2 f3 gamma gammal
global k1 k2 lc lambda lambda1 lambdac
global N ntv novs
global omega p
global psib R rA rcp rc rho rtf Rul Rux Ruy Ruz
global sigma
global T theta1 theta1R theta0 Treq V vh vx vy vz

```

```

global vzt vzi vzf

% CT2 : CT per unit length
% decfac : deciding factor
% T2 : T per unit length

theeta2 = (theta0 + theta1*(rcp-rc*R));
decfac = (lambdac/2+sigma*a/16)^2 + ...
    sigma*a/8*(theeta2.*rcp/R-lambdac);
if any(decfac<0.0)
    CT2(1:novs+ntv-1) = 0.003/R;
else
    lambdai2 = -(lambdac/2+sigma*a/16)+ ...
        sqrt((lambdac/2+sigma*a/16)^2 + ...
            sigma*a/8*(theeta2.*rcp/R-lambdac));
    lambda2 = lambdai2 + lambdac;
    CT2 = sigma*a/2*(theeta2.*(rcp/R).^2-lambda2.*rcp/R)*1/R;
end
T2 = CT2*rho*pi*R^2*(omega*R)^2;

gammal(1:novs+ntv-1) = 0;
gamma(1:novs+ntv) = 0;

gammal = T2./(rho*(omega*rcp));
for i = novs:novs+ntv-1
    gammal(i) = (rA(novs+ntv)-rcp(i))/(rA(novs+ntv)...
        -rcp(novs))*gammal(novs-1);
end
gamma(1)=-gammal(1);
gamma(novs+ntv)=gammal(novs+ntv-1);
for i = 2:novs+ntv-1
    gamma(i)=gammal(i-1)-gammal(i);
end

% *****

% Function to estimate Thrust Coefficient

function[CT1] = ThrCoe(theta0)
global a as A Ar C CL CD CQ CT f1 f2 f3 gamma gammal
global k1 k2 lc lambda lambdai lambdac
global N ntv novs
global omega p
global psib R rA rcp rc rho rtf Rul Rux Ruy Ruz
global sigma
global T thetai theta1R theta0 Treq V vh vx vy vz
global vzt vzi vzf

% non-uniform inflow
lambdac = V/(omega*R);
dr = [rc:(1.0-rc)/10:1.0];
CT1 = 0;
for i = 1:10
    CT1 = CT1 + quad1('dCT',dr(i),dr(i+1));
end

```

```
T = (T1*rho*pi*R^2*(omega^4*R)^2;
```

```
0.1) ****
```

```
" a function for thrust coefficient
```

```
function f = dCT(rb)
global a as A Ar C CL CD CQ CT f1 f2 f3 gamma gammal
global k1 k2 lc lambda lambdal lambdac
global N ntv novs
global omega p
global psib R rA rcp rc rho rtf Rul Rux Ruy Ruz
global sigma
global T theta1 theta1R theta0 Treq V vh vx vy vz
global vzt vzi vzf
```

```
% decfac : deciding factor
```

```
% rb : r/R
```

```
theeta = (theta0 + theta1*rb*R);
decfac = (lambdac/2+sigma*a/16)^2 + ...
         sigma*a/8*(theeta.*rb-lambdac);
if any(decfac<0.0)
    f = 0.003*rb./rb;
else
    lambdai = -(lambdac/2+sigma*a/16)+ ...
              sqrt((lambdac/2+sigma*a/16)^2 + ...
                  sigma*a/8*(theeta.*rb-lambdac));
    lambda = lambdai + lambdac;
    f = sigma*a/2*(theeta.*(rb).^2-lambda.*rb);
end
```

```
% ****
```

```
% Total Induced velocity calculation
```

```
function[vx,vy,vz]=TotInd(cc)
global a as A Ar C CL CD CQ CT f1 f2 f3 gamma gammal
global k1 k2 lc lambda lambdal lambdac
global N ntv novs
global omega p
global psib R rA rcp rc rho rtf Rul Rux Ruy Ruz
global sigma
global T theta1 theta1R theta0 Treq V vh vx vy vz
global vzt vzi vzf
```

```
[vxt,vyt,vzt]=IndTip(1); % tip-vortex contribution
[vxi,vyi,vzi]=IndInbV(1); % inboard-sheet contribution
[vxl,vyl,vzl]=IndLL(1); % other lifting-line contribution
[vxf,vyf,vzf]=IndFW(1); % far-wake contribution
vx = vxt+vxi+vxl+vxf;
vy = vyt+vyi+vyl+vyf;
vz = vzt+vzi+vzl+vzf;
```

```
%*****
```


% function for calculating the induced velocity due to tip-vortex

```
function[vxt,vyt,vzt] = IndTip(cc)
```

```
global a as A Ar C CL CD CQ CT f1 f2 f3 gamma gammat  
global k1 k2 lc lambda lambda1 lambda2  
global N ntv novs  
global omega p  
global psib R rA rep re rho rtf Rul Rux Ruy Ruz  
global sigma  
global T theta1 theta1R theta0 Treq V vh vx vy vz  
global vzt vzi vzf
```

```
vxt(1:novs+ntv-1)=0;vyt(1:novs+ntv-1)=0;vzt(1:novs+ntv-1)=0;  
% initialisation of induced velocities
```

```
for k = 0:N-1
```

```
% Lifting Line equation  
% assumption -> reference blade on y axis  
% assumption -> Rul < psib  
% rotating coordinate system chosen
```

```
gammat = 0;  
for i = novs+1:novs+ntv  
    gammat = gammat + gamma(i);  
end  
for l = 1:novs+ntv-1
```

```
    count = round((Rul-0)/as);  
    ang = [0+k*psib:(Rul-0)/count:Rul+k*psib]; % dividing the domain  
    for jj = 1:count  
        for i = 1:ntv  
            vxt(l) = vxt(l) + gamma(i+novs)/(4*pi)*quad1('px',ang(jj),ang(jj+1),[],[],i,1,k,1,1);  
            %vyt(l) = vyt(l) + gamma(i+novs)/(4*pi)*quad1('px',ang(jj),ang(jj+1),[],[],i,2,k,1,1);  
            vzt(l) = vzt(l) + gamma(i+novs)/(4*pi)*cos(sweep)*ang(jj),ang(jj+1),[],[],i,3,k,1,1);  
        end  
    end
```

```
    count = round((psib-Rul)/as);  
    ang = [Rul+k*psib:(psib-Rul)/count:psib+k*psib];  
    for jj = 1:count  
        vxt(l) = vxt(l) + gammat/(4*pi)*quad1('px',ang(jj),ang(jj+1),[],[],ntv,1,k,1,1);  
        %vyt(l) = vyt(l) + gammat/(4*pi)*quad1('px',ang(jj),ang(jj+1),[],[],ntv,2,k,1,1);  
        vzt(l) = vzt(l) + gammat/(4*pi)*cos(sweep)*ang(jj),ang(jj+1),[],[],ntv,3,k,1,1);  
    end
```

```
    count = round((4*psib-psib)/as);  
    ang = [psib+k*psib:(4*psib-psib)/count:4*psib+k*psib];  
    for jj = 1:count  
        vxt(l) = vxt(l) + gammat/(4*pi)*quad1('px',ang(jj),ang(jj+1),[],[],ntv,1,k,1,0);  
        %vyt(l) = vyt(l) + gammat/(4*pi)*quad1('px',ang(jj),ang(jj+1),[],[],ntv,2,k,1,0);  
        vzt(l) = vzt(l) + gammat/(4*pi)*cos(sweep)*ang(jj),ang(jj+1),[],[],ntv,3,k,1,0);  
    end  
end
```

end

v_n *****

v_n integrand for tip vortex induced velocities

function f = pv(psiw,i,j,k,l,flag)

global a as A Ar C CL CD CQ CT f1 f2 f3 gamma gammal

global k1 k2 lc lambda lambda1 lambda2

global N ntv novs

global omega p

global psib R rA rcp rc rho rtf Rul Rux Ruy Ruz

global sigma

global T thetal thetalR theta0 Treq V vh vx vy vz

global vzt vzi vzf

% i : tip vortex no.

% j : component (x=1,y=2,z=3)

% k : blade no.

% l : control pt. no.

% flag : just a no.

[Rux,Ruy,Ruz] = TipVor(Rul+k*psib,k);

if i==ntv

[xt(i,:),yt(i,:),zt(i,:)] = TipVor(psiw,k);

else

[xt(:,i),yt(:,i),zt(:,i)] = OthTV(psiw,k,i);

end

% Lifting Line equation

% assumption -> reference blade on y axis

% assumption -> Rul < psib

% rotating coordinate system chosen

if (i==ntv)&(psiw<=(Rul+k*psib))

dxt(i,:) = (-1/Rul)*rA(i+novs)*(-sin(k*psib))+Rux/Rul;

dzt(i,:) = (-1/Rul)*rA(i+novs)*cos(k*psib) + Ruy/Rul;

dzt(i,:) = Ruz/Rul;

else

dxt(i,:) = -R*(-lambda1)*(1-A)*exp(-lambda1*(psiw-k*psib))...

. *sin(psiw) - R*(A+(1-A)*exp(-lambda1*(psiw-k*psib)))...

. *cos(psiw) ;

dzt(i,:) = R*(-lambda1)*(1-A)*exp(-lambda1*(psiw-k*psib))...

. *cos(psiw) - R*(A+(1-A)*exp(-lambda1*(psiw-k*psib)))...

. *sin(psiw) ;

dzt(i,:) = -(R*k1);

end

if flag == 0

dzt(i,:) = -(R*k2);

end

r1(i,:) = sqrt((-rcp(l)*sin(0)-xt(i,:)).^2+...
(rcp(l)*cos(0)-yt(i,:)).^2+(-zt(i,:)).^2);

```

len = length(r1(i,:));
for ni = 1:len
    if r1(i,n) < 0.005*R
        r1(i,ni) = 0.005*R;          % to prevent singularity
    end
end

switch j
    case 1,
        f = -(dzt(i,:).*zt(i,:)+dzt(i,:).*(rcp(l)*cos(0)-yt(i,:)))/(r1(i,:).^3);
    case 2,
        f = (dzt(i,:).*(-rcp(l)*sin(0)-xt(i,:))+dxt(i,:).*zt(i,:))/(r1(i,:).^3);
    case 3,
        f = (dxt(i,:).*(rcp(l)*cos(0)-yt(i,:))-dzt(i,:).*...
            (-rcp(l)*sin(0)-xt(i,:)))/(r1(i,:).^3);
end

%%*****

% Function defining tip vortex geometry
% Parametric equations

function[xt5,yt5,zt5] = TipVor(psiw,k)

global a as A Ar C CL CD CQ CT f1 f2 f3 gamma gammad
global k1 k2 lc lambda lambda1 lambdac
global N ntv novs
global omega p
global psib R rA rcp rc rho rtf Rul Rux Ruy Ruz
global sigma
global T theta1 theta1R theta0 Treq V vh vx vy vz
global vzt vzi vzf

theta1R = theta1*(1-rc)*R*180/pi;
A = 0.78;
B = -0.000729*theta1R;
C1 = -2.3 + 0.206*theta1R;
m = 1.0 - 0.25*exp(0.040*theta1R);
n = 0.5-0.0172*theta1R;
k1 = (B + C1*(CT/N^n)^m)*(1.35-0.3/exp(V/vh));
CT0 = N^n*(-B/C1)^(1/m);
k2 = -(abs(CT-CT0))^0.5*(1.35-0.3/exp(V/vh));
lambda1 = 4.0*(CT)^0.5*(-0.35+0.47*(1.7+V/vh)^2);

xt5 = -R*(A+(1-A)*exp(-lambda1*(psiw-k*psib))).*sin(psiw);
yt5 = R*(A+(1-A)*exp(-lambda1*(psiw-k*psib))).*cos(psiw);

if (psiw>=(0+k*psib)&psiw<=(psib+k*psib))
    zt5 = -(R*k1*(psiw-k*psib));
elseif (psiw>=(psib+k*psib)&psiw<=(4*psib+k*psib))
    zt5 = -(R*(k1*psib+k2*(psiw-k*psib-psib)));
else
    zt5 = 0;
end

```

```

if psiw > 4*psib+k*psib
    xt5 = 0; yt5 = 0; zt5 = 0;
end

%*****

% Function defining tip vortex geometry
% Parametric equations

function[xt5,yt5,zt5] = TipVor(psiw,k)

global a as A Ar C CL CD CQ CT f1 f2 f3 gamma gammad
global k1 k2 lc lambda lambda1 lambdac
global N ntv novs
global omega p
global psib R rA rcp rc rho rtf Rul Rux Ruy Ruz
global sigma
global T theta1 theta1R theta0 Treq V vh vx vy vz
global vzt vzi vzf

theta1R = theta1*(1-rc)*R*180/pi;
A = 0.78;
B = -0.000729*theta1R;
C1 = -2.3 + 0.206*theta1R;
m = 1.0 - 0.25*exp(0.040*theta1R);
n = 0.5-0.0172*theta1R;
k1 = (B + C1*(CT/N^n)^m)*(1.35-0.3/exp(V/vh));
CT0 = N^n*(-B/C1)^(1/m);
k2 = -(abs(CT-CT0))^0.5*(1.35-0.3/exp(V/vh));
lambda1 = 4.0*(CT)^0.5*(-0.35+0.47*(1.7+V/vh)^2);

xt5 = -R*(A+(1-A)*exp(-lambda1*(psiw-k*psib))).*sin(psiw);
yt5 = R*(A+(1-A)*exp(-lambda1*(psiw-k*psib))).*cos(psiw);

if (psiw>=(0+k*psib)&psiw<=(psib+k*psib))
    zt5 = -(R*k1*(psiw-k*psib));
elseif (psiw>=(psib+k*psib)&psiw<=(4*psib+k*psib))
    zt5 = -(R*(k1*psib+k2*(psiw-k*psib-psib)));
else
    zt5 = 0;
end

if psiw > 4*psib+k*psib
    xt5 = 0; yt5 = 0; zt5 = 0;
end

%*****

% Equations of other tip vortices

function[xt,yt,zt] = OthTV(psiw,k,i)

global a as A Ar C CL CD CQ CT f1 f2 f3 gamma gammad
global k1 k2 lc lambda lambda1 lambdac
global N ntv novs
global omega p

```

```

global psib R rA rcp rc rho rtf Rul Rux Ruy Ruz
global sigma
global T theta1 theta1R theta0 Treq V vh vx vy vz
global vzt vzi vzf

```

```

t = (psiw-k*psib)/Rul;

```

```

if psiw < (Rul+k*psib)
    xt(i,:) = (1-t)*rA(i+novs)*(-sin(k*psib)) + t*Rux;
    yt(i,:) = (1-t)*rA(i+novs)*cos(k*psib) + t*Ruy;
    zt(i,:) = t*Ruz;

```

```

elseif (psiw>(Rul+k*psib)&psiw<=(psib+k*psib))
    xt(i,:) = -R*(A+(1-A)*exp(-lambda1*(psiw-k*...
        psib))).*sin(psiw);
    yt(i,:) = R*(A+(1-A)*exp(-lambda1*(psiw-k*...
        psib))).*cos(psiw);
    zt(i,:) = -(R*k1*(psiw-k*psib));
elseif (psiw>(psib+k*psib)&psiw<=(4*psib+k*psib))
    xt(i,:) = -R*(A+(1-A)*exp(-lambda1*(psiw-...
        k*psib))).*sin(psiw);
    yt(i,:) = R*(A+(1-A)*exp(-lambda1*(psiw-...
        k*psib))).*cos(psiw);
    zt(i,:) = -(R*(k1*psib + k2*(psiw-k*psib-psib)));
else
    xt(i,:) = 0;
    yt(i,:) = 0;
    zt(i,:) = 0;
end

```

```

% *****

```

```

% Induced velocities due to Inboard Vortices

```

```

function[vxi,vyi,vzi] = IndInbV(cc)

```

```

global a as A Ar C CL CD CQ CT f1 f2 f3 gamma gammal
global k1 k2 lc lambda lambda1 lambda2
global N ntv novs
global omega p
global psib R rA rcp rc rho rtf Rul Rux Ruy Ruz
global sigma
global T theta1 theta1R theta0 Treq V vh vx vy vz
global vzt vzi vzf

```

```

vxi(1:novs+ntv-1)=0;vyi(1:novs+ntv-1)=0;vzi(1:novs+ntv-1)=0;

```

```

if psib>pi/2
    ang1 = pi/2;ang2 = psib;
else
    ang1 = psib;ang2 = pi/2;
end
for k = 0:N-1
    count1 = round(ang1/as);
    anga = [0+k*psib:ang1/count1:ang1+k*psib];
    count2 = round((ang2-ang1)/as);

```

```

if (ang1 == ang2)
    angb(1:count2) = 0;
else
    angb = [ang1 + k*psib*(ang2-ang1)/count2:ang2+k*psib];
end
count3 = round((4*psib-ang2)/as);
angc = [ang2+k*psib:(4*psib-ang2)/count3:4*psib+k*psib];

for l = 1:novs+ntv-1
    for jj = 1:count1
        for i = 1:novs
            vxi(l) = vxi(l) + gamma(i)/(4*pi)*quad1('qx',anga(jj),anga(jj+1),[],[],i,1,k,1,0);
            %vyi(l) = vyi(l) + gamma(i)/(4*pi)*quad1('qx',anga(jj),anga(jj+1),[],[],i,2,k,1,0);
            vzi(l) = vzi(l) + gamma(i)/(4*pi)*quad1('qx',anga(jj),anga(jj+1),[],[],i,3,k,1,0);
        end
    end
    for jj = 1:count2
        for i = 1:novs
            vxi(l) = vxi(l) + gamma(i)/(4*pi)*quad1('qx',angb(jj),angb(jj+1),[],[],i,1,k,1,1);
            %vyi(l) = vyi(l) + gamma(i)/(4*pi)*quad1('qx',angb(jj),angb(jj+1),[],[],i,2,k,1,1);
            vzi(l) = vzi(l) + gamma(i)/(4*pi)*quad1('qx',angb(jj),angb(jj+1),[],[],i,3,k,1,1);
        end
    end
    for jj = 1:count3
        for i = 1:novs
            vxi(l) = vxi(l) + gamma(i)/(4*pi)*quad1('qx',angc(jj),angc(jj+1),[],[],i,1,k,1,2);
            %vyi(l) = vyi(l) + gamma(i)/(4*pi)*quad1('qx',angc(jj),angc(jj+1),[],[],i,2,k,1,2);
            vzi(l) = vzi(l) + gamma(i)/(4*pi)*quad1('qx',angc(jj),angc(jj+1),[],[],i,3,k,1,2);
        end
    end
end
end
end
end

```

```

%*****
*****

```

% integrand for inboard vortex induced velocities

```
function f = qx(psi,i,j,k,l,flag)
```

```

global a as A Ar C CL CD CQ CT f1 f2 f3 gamma gammal
global k1 k2 lc lambda lambda1 lambda2
global N ntv novs
global omega p
global psib R rA rcp rc rho rtf Rul Rux Ruy Ruz
global sigma
global T theta1 theta1R theta0 Treq V vh vx vy vz
global vzt vzi vzf

```

% i : vortex no.

% j : component (x=1,y=2,z=3)

% k : blade no.

% l : control pt. no.

% flag : just a no.

```

k20 = (theta1R+128*(0.45*theta1R+18))*sqrt(CT/2);
k11 = -2.2*sqrt(CT/2)*(1.35-0.3/exp(V/vh));
k21 = -2.7*sqrt(CT/2)*(1.35-0.3/exp(V/vh));
switch flag
case 0,
    zi(i,:) = -(k11*(psi-k*psib)*rA(i));
    dzi(i,:) = -(k11*rA(i));

case 1,
    if psib > pi/2
        zi(i,:) = -(k20*(psi-k*psib-pi/2)*R+(k11*...
            (psi-k*psib)-k20*(psi-k*psib...
            -pi/2))*rA(i));
        dzi(i,:) = -(k20*R+(k11-k20)*rA(i));
    else
        zi(i,:) = -(k11*psib+k21*(psi-k*psib-psib))...
            *rA(i);
        dzi(i,:) = -(k21*rA(i));
    end
case 2
    zi(i,:) = -(R*k20*(psi-k*psib-pi/2)+...
        (k11*psib+k21*(psi-k*psib-psib)-...
        k20*(psi-k*psib-pi/2))*rA(i));
    dzi(i,:) = -(R*k20+(k21-k20)*rA(i));
end

if zi(i,:) == 0.0
    psiw = 0.0;
elseif (zi(i,:) < -(k1*psib*R)) & (zi(i,:) ~= 0.0)
    psiw = -zi(i,)/(R*k1)+k*psib;
else
    psiw = (-zi(i,)/R-k1*psib)/k2 + psib + k*psib;
end

if psiw > 8*pi/N+k*psib
    psiw = 8*pi/N+k*psib;
end

rt = R*(A+(1-A)*exp(-lambda1*(psiw-k*psib)));
rad = rA(i)*rt/R;
xi(i,:) = -rad.*sin(psi);
yi(i,:) = rad.*cos(psi);

dxi(i,:) = -rad.*cos(psi);
dyi(i,:) = -rad.*sin(psi);

r2(i,:) = sqrt((-rcp(l)*sin(0)-xi(i,:)).^2+(rcp(l)*cos(0)-yi(i,:)).^2+...
    +(-zi(i,:)).^2);

len = length(r2(i,:));
for iii = 1:len
    if r2(i,iii) < 0.005*R
        r2(i,iii) = 0.005*R; % to prevent singularity
    end
end
end

```

```

switch j
    case 1,
        f = -(dyi(i,:).*zi(i,:)+dzi(i,:).*(rcp(l)*cos(0)-yi(i,:)))/(r2(i,:).^3);
    case 2,
        f = (dzi(i,:).*(-rcp(l)*sin(0)-xi(i,:))+dxi(i,:).*zi(i,:))/(r2(i,:).^3);
    case 3,
        f = (dxi(i,:).*(rcp(l)*cos(0)-yi(i,:))-dyi(i,:).*(-rcp(l)*sin(0)-xi(i,:)))/(r2(i,:).^3);
end

```

%

```

%*****
%*****

```

% Induced velocities due to other Lifting Lines

```

function[vxl,vyl,vzl]=IndLL(cc)

```

```

global a as A Ar C CL CD CQ CT f1 f2 f3 gamma gammal
global k1 k2 lc lambda lambda1 lambdac
global N ntv novs
global omega p
global psib R rA rcp rc rho rtf Rul Rux Ruy Ruz
global sigma
global T theta1 theta1R theta0 Treq V vh vx vy vz
global vzt vzi vzf

```

```

vxl(1:novs+ntv-1)=0;vyl(1:novs+ntv-1)=0;vzl(1:novs+ntv-1)=0;

```

```

for k = 1:N-1
    for l = 1:novs+ntv-1
        for i = 1:novs+ntv-1
            vzl(l) = vzl(l)+gammal(i)/(4*pi)*quad1('sx',rA(i),rA(i+1),[],[],k,l);
        end
    end
end
end

```

% note : x & y components are zero

```

%*****

```

% integrand for lifting line induced velocities

```

function f = sx(m,k,l)

```

```

global a as A Ar C CL CD CQ CT f1 f2 f3 gamma gammal
global k1 k2 lc lambda lambda1 lambdac
global N ntv novs
global omega p
global psib R rA rcp rc rho rtf Rul Rux Ruy Ruz
global sigma
global T theta1 theta1R theta0 Treq V vh vx vy vz
global vzt vzi vzf

```

% k : blade no.

% l : no. of control pt.


```
r1 = sqrt((-rcp(l)*sin(0)+m*sin(0+k*psib)).^2 + ...
    (rcp(l)*cos(0)-m*cos(0+k*psib)).^2);
```

```
dlx = -sin(0+k*psib);
dly = cos(0+k*psib);
dlz = 0;
```

```
% x & y components of ind vel = 0
```

```
f = (dlx.*(rcp(l)*cos(0)-m*cos(0+k*psib))-...
    dly.*(-rcp(l)*sin(0)+m*sin(0+k*psib))./(r1.^3);
```

```
%*****
```

```
% Induced velocity due to Far Wake
```

```
function[vxf,vyf,vzf]=IndFW(cc)
```

```
global a as A Ar C CL CD CQ CT f1 f2 f3 gamma gammad
global k1 k2 lc lambda lambda1 lambdac
global N ntv novs
global omega p
global psib R rA rcp rc rho rtf Rul Rux Ruy Ruz
global sigma
global T theta1 theta1R theta0 Treq V vh vx vy vz
global vzt vzi vzf
```

```
vxf(1:novs+ntv-1) = 0;vyf(1:novs+ntv-1) = 0;vzf(1:novs+ntv-1) = 0;
gammat = 0;
for i = novs+1:novs+ntv
    gammat = gammat + gamma(i);
end
count = round(6.2832/as);
ang = [0:6.2832/count:6.2832];
```

```
for jj =1:count
    for l = 1:novs+ntv-1
        vxf(l) = vxf(l) + 8*gammat/(4*pi)*quad1('rx',ang(jj),ang(jj+1),[],[],1,l);
        %vyf(l) = vyf(l) + gammat/pi*quad1('rx',ang(jj),ang(jj+1),[],[],2,l);
        vzf(l) = vzf(l) + 8*gammat/(4*pi)*quad1('rx',ang(jj),ang(jj+1),[],[],3,l);
    end
end
```

```
%*****
```

```
% integrand for far wake induced velocities
```

```
function f = rx(phi,j,l)
```

```
global a as A Ar C CL CD CQ CT f1 f2 f3 gamma gammad
global k1 k2 lc lambda lambda1 lambdac
global N ntv novs
global omega p
global psib R rA rcp rc rho rtf Rul Rux Ruy Ruz
global sigma
global T theta1 theta1R theta0 Treq V vh vx vy vz
```

```

global vzt vzi vzf

% j : component (x=1,y=2,z=3)
% l : control pt. no.

[xth,yth,zth] = TipVor(4*psib,0);

l1=4.0*(CT)^0.5;
rr1=R*(A+(1-A)*exp(-l1*8*pi/N)); % radius of the tipvortex in hover
l2=4.0*(CT)^0.5*(-0.35+0.467*(1.7+V/vh).^2);
rr2=R*(A+(1-A)*exp(-l2*8*pi/N)); % radius in axial flight

xf=-rr2/rr1*R*sin(phi+0);
yf=rr2/rr1*R*cos(phi+0);
zf=zth;

rlx(l,:)=-rcp(l)*sin(0)-xf;
rly(l,:)=rcp(l)*cos(0)-yf;
rlz(l,:)=-zf;
rl(l,:)=sqrt(rlx(l,:).^2+rly(l,:).^2+rlz(l,:).^2);

dlx=-rr2/rr1*R*cos(phi+0);
dly=-rr2/rr1*R*sin(phi+0);
dlz=0;
switch j
case 1,
    f=(dly.*rlz(l,:)-dlz.*rly(l,:))/(rl(l,:).^3);
case 2,
    f=(dlz.*rlx(l,:)-dlx.*rlz(l,:))/(rl(l,:).^3);
case 3,
    f=(dlx.*rly(l,:)-dly.*rlx(l,:))/(rl(l,:).^3);
end

%*****

% Computation of gamma values

function[gamma]=Compgam(cc)

global a as A Ar C CL CD CQ CT f1 f2 f3 gamma gammal
global k1 k2 lc lambda lambda1 lambdac
global N ntv novs
global omega p
global psib R rA rcp rc rho rtf Rul Rux Ruy Ruz
global sigma
global T theta1 theta1R theta0 Treq V vh vx vy vz
global vzt vzi vzf

flagg=1;countt=0;
while flagg==1

for i=1:novs+ntv-1
    u(i)=omega*rcp(i);
    f1=V+vz(i);
    f2=-(u(i)+vx(i));
    f3=sqrt(f1.^2+f2.^2);

```

```

    gammaln(i) = a*C*f3/2.*(theta0+theta1*(rcp(i)-rc*R)-atan(f1/f2));
end

flaggl = 0;
for i = 1:novs+ntv-1
    if abs(gammaln(i)-gammal(i))>(0.1*gammaln(i))
        flaggl = 1;
    end
    gammal(i) = gammal(i)+0.1*(gammaln(i)-gammal(i));
end

gamma(1)=-gammal(1);
gamma(novs+ntv)=gammal(novs+ntv-1);
for i = 2:novs+ntv-1
    gamma(i)=gammal(i-1)-gammal(i);
end

if flaggl == 0
    flagg = 0; break;
end
[vx,vy,vz]=TotInd(1);
end

%*****

% Performance calculations

function[CT,CQ,alpha] = PerCal(cc)

global a as A Ar C CL CD CQ CT f1 f2 f3 gamma gammal
global k1 k2 lc lambda lambda1 lambdac
global N ntv novs
global omega p
global psib R rA rcp rc rho rtf Rul Rux Ruy Ruz
global sigma
global T theta1 theta1R theta0 Treq V vh vx vy vz
global vzt vzi vzf

% Calculate angle of attack

alpha(1:novs+ntv-1) = 0;

for i = 1:novs+ntv-1
    u(i) = omega*rcp(i);
    f1 = V+vz(i);
    f2 = -(u(i)+vx(i));
    f3 = sqrt(f1.^2 + f2.^2);
    alpha(i) = 2*gammal(i)/(a*C*f3);
    CL(i) = ppval(lc,alpha(i));
    CD(i) = ppval(p,CL(i));
    mu(i) = CD(i)/CL(i);
    drcp(i) = rA(i+1)-rA(i);
    gammab(i) = gammal(i)/(omega*R^2);
end
sum1 = 0; sum2 = 0;
for i = 1:novs+ntv-1

```

```

if CT(i) == 0
    sum1 = sum1 + (-CT(i)*(V+vx(i))^(omega*R))...
            *t.*C'*u(i)^(omega*R^2)*drcp(i)/R;
    sum2 = sum2 + (CT(i)*(rcp(i)/R-vx(i)^(omega*R)))...
            *t.*C'*u(i)^(omega*R^2)*rcp(i)/R*drcp(i)/R;
else
    sum1 = sum1 + (rcp(i)/R-vx(i)/(omega*R)-mu(i)*(V+vx(i))...
            (omega*R))*gammab(i)*drcp(i)/R;
    sum2 = sum2 + ((V+vx(i)/(omega*R)+mu(i)*(rcp(i)/R-vx(i))...
            (omega*R))*gammab(i)*rcp(i)/R*drcp(i)/R;
end
end

CT = N*pi*sum1;
CQ = N*pi*sum2;

a = *****
(0)

```

A...

